Secondary Prevention for Alzheimer Disease

Vermunt, L.

2020

document version
Publisher's PDF, also known as Version of record

4

Chapter 4

Grey matter networks, a potential endpoint for trials

Chapter 4.1

Grey matter networks decline over the disease course of autosomal dominant Alzheimer disease

Lisa Vermunt, Ellen Dicks, Guoqiao Wang, Aylin Dincer, Shaney Flores, Sarah J. Keefe, Sarah B. Berman, David M. Cash, Jasmeer P. Chhatwal, Carlos Cruchaga, Nick C. Fox, Bernardino Ghetti, Neill R. Graff-Radford, Jason Hassenstab, Celeste M. Karch, Christoph Laske, Johannes Levin, Colin L. Masters, Eric McDade, Hiroshi Mori, John C. Morris, James M. Noble, Richard J. Perrin, Peter R. Schofield, Chengjie Xiong, Philip Scheltens, Pieter Jelle Visser, Randall J. Bateman, Tammie L.S. Benzinger, Betty M. Tijms, Brian A. Gordon, on behalf of the Dominantly Inherited Alzheimer Network (DIAN).

As submitted for publication

Abstract

INTRODUCTION: Structural grey matter covariance networks provide an individual quantification of morphological patterns in the brain. These networks are disrupted in sporadic Alzheimer disease, and show associations with early Alzheimer disease pathological changes and cognitive decline. Therefore, these networks might be disease progression markers. However, it remains unclear when and how grey matter networks change with disease progression. We investigated these questions in autosomal dominant Alzheimer disease mutation carriers, whose conserved age at dementia onset allows individual staging based upon their estimated years to symptom onset.

METHODS: From the Dominantly Inherited Alzheimer Network observational cohort, we selected T1-weighted MRI scans from 269 mutation carriers and 170 non-carriers (mean age 38±15 years, mean estimated years to symptom onset -9±11), of whom 237 had longitudinal scans with a mean follow-up of 3.0 years. Single-subject grey matter networks were extracted, and we calculated for each individual the network properties which describe the network topology, including the size, clustering, path length and small worldness. We determined at which time point mutation carriers and non-carriers diverged for global and regional grey matter network metrics, both cross-sectionally and for rate of change over time.

RESULTS: Based on cross-sectional data, the earliest difference was observed in path length which was decreased for mutation carriers in the precuneus area at 13 years and on a global level 12 years before estimated symptom onset. Based on longitudinal data, we found the earliest difference between groups on a global level 6 years before symptom onset, with a greater rate of decline of network size for mutation carriers. We further compared grey matter network measures with established biomarkers for AD (i.e., amyloid accumulation, cortical thickness, brain metabolism, and cognitive function). We found that greater amyloid accumulation at baseline was associated with faster decline of network measures over time, and decline in grey matter network measures over time was accompanied by decline in brain metabolism, cortical thinning, and cognitive decline.

CONCLUSION: In summary, grey matter networks deteriorate in autosomal dominant Alzheimer disease in a similar fashion as in sporadic Alzheimer disease, and the network measures show decline over time prior to estimated symptom onset. These data suggest that single-subject networks obtained from structural MRI scans form an additional non-invasive tool for understanding the substrate of cognitive decline and measuring progression from preclinical to severe clinical stages of Alzheimer disease.

1 Introduction

In order to advance clinical trials to slow or halt Alzheimer disease, the most frequent cause of dementia [1], it is important both to understand the evolution of pathophysiological changes occurring and to develop disease progression markers [2]. Current biomarkers reliably detect Alzheimer disease pathology [3], however predicting and monitoring disease progression remains difficult. Brain networks are linked to cognitive function [4-6], and may offer insights into disease progression in Alzheimer disease.

One way to measure of brain networks is by determining the similarity of grey matter morphological measures between brain regions across individuals, i.e., grey matter covariance networks [7-9] (Panel 1). This approach is based on the notion that brain regions involved in distinct cognitive functions tend to develop in a similar way, possibly due to shared neurotrophic factors [10-12]. Common developmental trajectories and functional coactivation result in similar grey matter tissue properties, as measured on structural MR imaging [13-15]. These covariance patterns are related to normal cognition [16, 17], and reveal in healthy individuals an optimal, 'small-world', organization by graph theory description [18, 19]. In sporadic Alzheimer disease dementia, grey matter networks are disrupted, showing a less optimal, random organization [20-22]. In predementia stages, such network disruptions predict clinical progression and cognitive decline [23, 24]. The presence of amyloid β (Aβ) pathology in cognitively normal individuals has also been associated with grey matter network alterations [25-27]. Together, these observations suggest that these networks change over the course of Alzheimer disease, from early stages, and that individual grey matter networks could possibly be used to monitor disease progression. However, as previous findings were based on one-time grey matter network extractions, it remains unclear whether, and when, these networks change within individuals as they progress in their disease.

A complication when studying sporadic Alzheimer disease is the difficulty of placing presymptomatic individuals on their disease timeline [28-32]. This issue is less problematic for carriers of a genetic mutation that causes autosomal dominant Alzheimer disease, because the age at onset of dementia can be estimated, from the age at onset in family members or carriers of the same specific mutation type. The estimated years to symptom onset (EYO) can serve as a proxy for disease duration [33, 34]. Using this paradigm, previous work demonstrated that Aβ aggregation starts more than two decades before dementia onset [35-37]. Closer to symptom onset, individuals show accelerated hypometabolism and cortical thinning, which is followed by cognitive decline [38-40]. When during these processes grey matter networks start to decline remains unknown.

Here, we investigated for the first time single-subject grey matter networks over the course of autosomal dominant Alzheimer disease. We assessed when, and how, the networks change as a function of EYO, both cross-sectionally and longitudinally, on a global and regional level. To understand the relationship between grey matter network changes and disease progression, we also investigated how the networks alter with established Alzheimer disease markers.

2 Materials and methods

2.1 DIAN study design and participants

In the worldwide Dominantly Inherent Alzheimer Network (DIAN) longitudinal cohort study, families with individuals carrying a PSEN1, PSEN2 or APP mutation undergo genetic testing and repeated clinical, cognitive, fluid, and brain imaging assessments. The non-carrier family members act as an inherent control group. Participants generally have study visits every three years at earlier disease stages and these assessments become yearly when either symptoms are present, or they are within three years of their EYO. DIAN protocols had supervisory approval from the ethical review board of Washington University in St. Louis, and all participants gave informed consent. For this study, we selected data from all participants who had undergone at least one MRI scan that passed quality control in the 12th data freeze. Families with the Dutch or Flemish APP mutation were excluded because these mutations result in a different phenotype, with predominantly cerebral amyloid angiopathy.

2.2 Estimated years to symptom onset (EYO)

We calculated the EYO for mutation carriers and non-carriers identically: The EYO was defined as the mutation-specific mean age at onset subtracted by the individuals' visit age [34]. In case of an unknown mutation-specific age at onset, the parental age at disease onset, reported by the participant, was used instead. For example, if the mean age at symptom onset for a specific mutation is 50 years, then a 35 year old individual would have an EYO of -15. For the carriers of the ADAD mutation, this indicates that the individual is expected to show clinical symptoms of Alzheimer disease 15 years later.

2.3 Clinical evaluation and cognition

Disease severity was measured using the Clinical Dementia Rating scale (CDR) [41], administered to the participant and study partner by blinded raters. Participants were classified as being unimpaired (global CDR score=0) or symptomatic (global CDR 0.5, 1, 2 & 3). In addition, cognitive function was summarized using a cognitive composite developed in the DIAN project [42], consisting of the average of equally weighted z-scores of the Logical Memory delayed recall total score from the Wechsler Memory Scale-Revised, DIAN Word List Test delayed free recall score, Digit Symbol Coding total score from the Wechsler Adult Intelligence Scale-Revised Digit Symbol Substitution Test, and the total score from the Mini Mental State Examination.

2.4 MR imaging acquisition and preprocessing

MRI T1-weighted scans (1.1 x 1.1 x 1.2 mm3 voxels, repetition time = 2300 ms, echo time = 2.95 ms, flip angle 9°) were acquired according to Alzheimer Disease Neuroimaging Initiative (ADNI) protocols [43]. We segmented T1 images into grey and white matter and CSF, using the Statistical Parametric Mapping software version

12 (SPM12; Wellcome Trust Centre for Neuroimaging, UCL Institute of Neurology, London, UK). All segmentations were checked visually, after which 51 scans were removed due to failed segmentations or severe motion artifacts. Native space grey matter segmentations were resampled into 2 x 2 x 2 mm3 voxels. This voxel-wise data was used as input for connectivity analyses.

2.5 Single-subject Grey Matter Networks and Metrics

Grey matter networks were computed according to a previously published, automated pipeline [7] that includes two steps figurated in Panel A: (1) grey matter network extraction (https://github.com/bettytijms/Single_Subject_Grey_Matter_Networks; implemented in Matlab2016b (MathWorks, Natick, MA)), and (2) graph theory-based metric calculation [7, 44]. To extract single-subject grey matter networks, we parcellated each individual's native space grey matter segmentation into 6 x 6 x 6 mm3 cubes, containing 27 voxels. These non-overlapping cubes serve as the 'nodes' in the network. Connections between each pair of cubes across an individual's scan were established by calculating the Pearson's correlation coefficient between the corresponding voxels. This approach takes into account both the grey matter probability (i.e. from the tissue segmentation) as well as the spatial information present in 27 voxels within each cube. All correlations were stored in a matrix, and the presence or absence of connections between nodes was dichotomized according to an individualized threshold that ensured a maximum of 5% spurious connections for each individual [7].

For each individual's binarized grey matter network, we calculated graph theory metrics describing the global network properties: size, degree, connectivity density, clustering coefficient, path length, normalized clustering, normalized path length, and small world coefficient (see Panel 1 for explanation of these metrics). We also calculated regional network properties. In order to aid comparability with other studies previously performed in DIAN, regional network metrics were calculated within each region of the Desikan-Killiany atlas [45]. The regional masks were obtained by first parcellating each individual's T1 image into 34 anatomical regions of interest (ROIs) from the Desikan atlas using Freesurfer 5.3 [46] (http://surfer.nmr.mgh.harvard.edu). The Freesurfer output was then aligned to the native space T1 using FSL (https://fsl.fmrib.ox.ac.uk/fsl), and this transform was used to register the parcellation into native space. The network values of the degree, clustering coefficient, and path length were subsequently averaged within a region. Graph theory metrics were calculated using scripts from the brain connectivity toolbox (https://sites.google.com/site/bctnet/),

Panel 1 Grey matter network metrics

A. Grey matter network extraction from the individual brain segmentation (described in text)

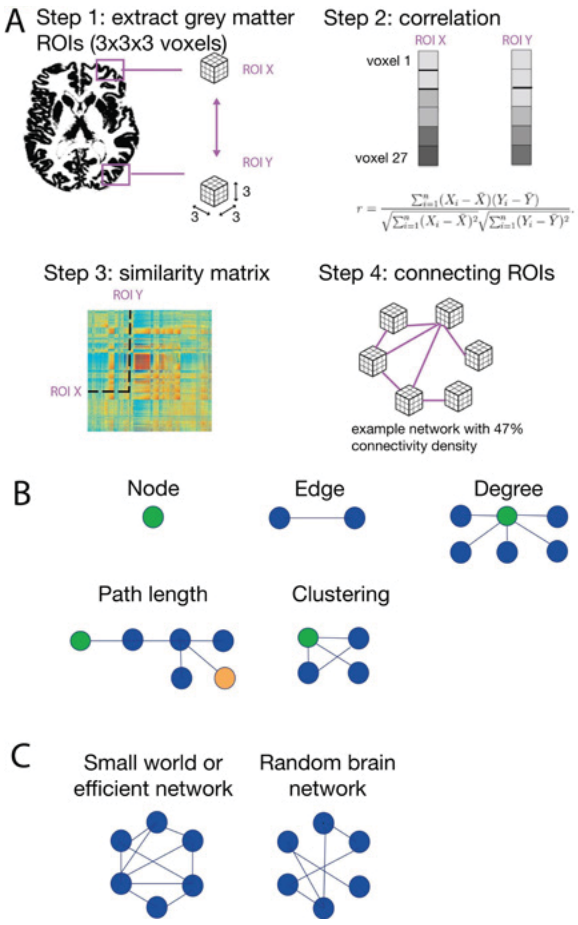

B. The sum of the number of nodes, i.e., the number of cubes, is the size of the network. The degree is the average number of connections per node. The connectivity density is the percentage of the number of connections in the network compared to the maximum number of connections possible. The clustering coefficient of a node describes the proportion of connections between neighbors for every node. For example, in case a node connects to 3 other nodes, there are 3 possible connections between those 3 adjacent nodes. If only 1 connection is present between 2 of the 3 other nodes, the clustering of the primary node is 1 out of 3, 0.33. Global clustering is determined by taking averaging clustering values across all nodes. Path length is the mean of the shortest paths for a node to reach every other node in the network. The global path length is the average path length across all nodes.

C. Normalized clustering and normalized path length describe how on a global level a network organization differs from a randomly organized network. The networks are randomized by rewiring the connections randomly in each network, while keeping intact the total number of nodes and degrees [47]. The network's observed clustering and path length are divided by the clustering and path length values, respectively, of averaged random networks to obtain the normalized values. Lastly, the small world coefficient is the normalized clustering divided by the normalized path length. The network has the "small world property" if this ratio is higher than 1, indicating a path length close to the random networks, yet a greater then random clustering. This is optimal, because of fast exchange of information between remote clusters, and specialized information processing within clusters.

(Picture adapted from Verfaillie, HBM 2018, with permission)

2.6 Other DIAN imaging data

We examined regional data for Aβ using PET imaging with 11C-Pittsburgh Compound B (Aβ PET), glucose metabolism with 18F-Fluorodeoxyglucose PET (FDG-PET), and cortical thickness and volumes from structural MRI. Details on data processing have previously been described [36]. The Freesurfer ROIs were used to process the amyloid and FDG-PET data. PET data are processed using a cerebellar grey reference region and partial volume corrected using a geometric transfer matrix approach [48, 49]. In this study, we utilized the MRI precuneus cortical thickness, the precuneus Aβ PET, and to match a previously defined meta-ROI, the average of the left and right isthmus cingulate and inferior parietal region in FDG-PET for crossmodal comparison with grey matter network properties [50].

2.7 Statistical analyses

We compared mutation carriers and non-carriers to determine (1) the EYO at which grey matter network metrics showed cross-sectional differences between groups, and (2) the EYO at which the groups had a different rate of change over time by fitting linear mixed effects models. Specifically, we used Bayesian inference methods [36, 51] to determine the EYO point that 99% credible intervals of the difference distribution did not overlap 0. To allow for non-linear effects, without assuming a particular shape, we applied a restricted cubic spline with knots at the 0.10, 0.50 and 0.90 of the EYO distribution, also described previously [36], that included a linear term (EYOlinear) and a cubic term (EYOcubic). Cross-sectional models contained fixed terms for EYO, mutation status, their interaction, and a random effect for family cluster. Longitudinal models included fixed terms for baseline EYO (two terms: EYOlinear and EYOcubic), time after baseline, mutation status and, all 2- and 3-way interactions (see formulas in Sup., p.6). Additionally, the models included random intercept terms for subject and family cluster, and a random slope for subject. The covariates whole-brain grey matter volume and sex were included as fixed terms. Equivalent to previous work, when size, degree or connectivity density were found to be associated with mutation status in any of the models, they were included as additional covariate as these variables also influence more complex network metrics [21]. Regional models were additionally adjusted for regional grey matter volume. Model parameters were estimated as previously described, applying a Hamiltonian Markov chain Monte Carlo sampling of the posterior distribution, with 10,000 iterations in 8 chains, thinning retaining 1 out of every 10 iterations, and cauchy prior in the STAN package for R [52, 53].

We examined relationships between grey matter networks and established AD markers within mutation carriers. Previous research suggested grey matter networks may be disrupted in response to Aβ accumulation, precipitating cognitive decline [26]. For this reason, our models included either precuneus PET Aβ as a predictor and grey matter network metrics as outcomes, or grey matter network metrics as a predictor and cortical thickness (precuneus), brain metabolism (meta-ROI), or cognition (DIAN cognitive composite) as the respective outcomes. These predictors and outcomes

were z-scored to the whole group. We fitted three sets of linear mixed effects models that were all adjusted for baseline grey matter volume, age, and sex, and with random intercept for family cluster, in lme4 package in R [54] (see detailed formulas in Sup., p.6). If models failed to converge, the term for family cluster was removed. Models were divided into three sections. The first were baseline comparisons. The second set were longitudinal comparisons in participants with at least 2 data points, and included additional random effects for subject intercept and slope of the predictor. The final set of models were used to evaluate whether baseline data could predict change over time in the outcome. These models had fixed effects for baseline predictor, time from baseline, and its interaction, and a random subject intercept and slope of time from baseline. We focused on the grey matter network small world coefficient, as this metric is indirectly derived from all other network metrics, and can thus be considered a summary statistic (Panel 1 p.8).

2.8 Data availability

The data of the study can be freely requested online at https://dian.wustl.edu/

3 Results

In total, 439 participants from the DIAN study, with a mean±SD age of 38±11 years and a mean±SD EYO of -9±11), had MRI scans of sufficient quality to be included in the present analyses. The group consisted of 269 (61%) ADAD mutation carriers and 170 (39%) non-carrier family members (Table 1). Of this sample, 237 (54%) participants had longitudinal MRI scans, with a mean of 2.5 scans per participant and a maximum of 6 acquired over a mean±SD 3.0±1.5 years of follow-up (clinical and PET data in Sup. Table S1).

Table 1 Group characteristics

	Non-carriers (n=170)	Asymptomatic mutation carriers (n=174)	Symptomatic mutation carriers (n=95)
Baseline age, years	38 (11)	34 (9)	46 (10)
Female, n (%)	101 (59%)	100 (57%)	50 (53%)
Estimated years to onset	-11 (12)	-14 (8)	1 (7)
MMSE	29.1 (1.2)	29.1 (1.2)	22.9 (6.6)
Total MR scans, 1/2/3/4-6, n	84/61/18/7	84/59/28/3	34/30/17/14
Follow-up time MR visits, years	3.3 (1.5)	3.2 (1.5)	2.2 (1.3)

Mean (SD), unless otherwise specified. MMSE=Mini Mental State Examination. Estimated years to symptom onset is the expected age at onset of the mutation that runs in the family.

3.1. Cross-sectional divergences between mutation carriers and non-carriers

The mutation carriers diverged from non-carriers on all grey matter network metrics, except for network size and raw path length (Figure 1, Sup. Table S2). Lower network metric values for mutation carriers relative to non-carriers were observed earliest in normalized path length at EYO -12, followed by lower normalized clustering at EYO -8.7, small world coefficient at EYO -8.4, clustering coefficient at EYO -7.5, connectivity density at EYO -5.6, and degree at EYO 0. Using the same methods, but now implemented on a regional level, the earliest divergence between mutation carriers relative to non-carriers was found for path length in the precuneus at EYO -13.1, for clustering in the superior temporal gyrus at EYO -10, and for network degree in the banks of the superior temporal gyrus at EYO -7 (Figure 3, Sup. Table S3).

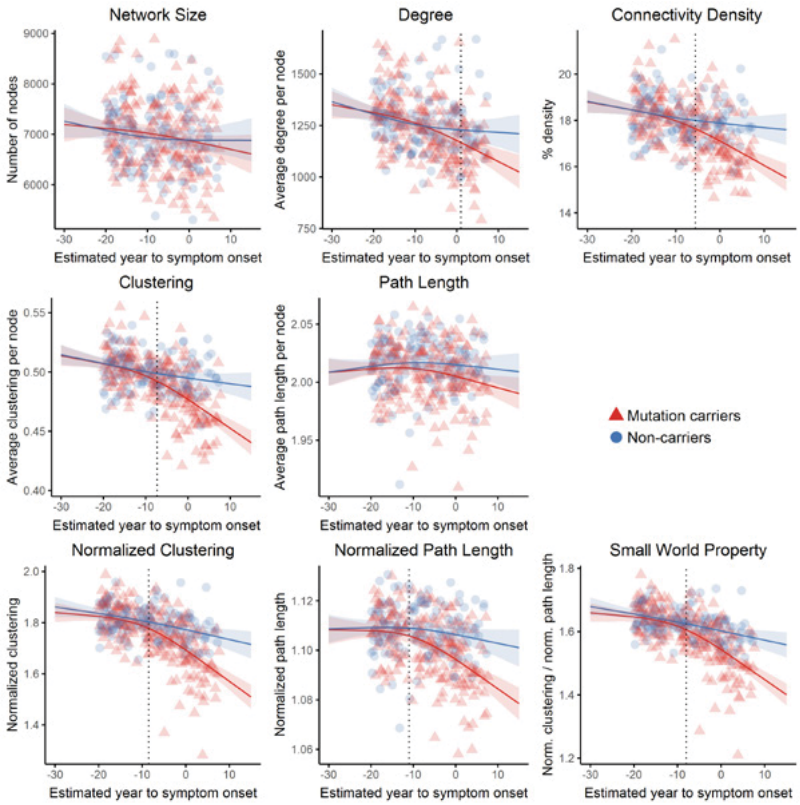

Figure 1 Grey matter networks by estimated year of onset at baseline between mutation carriers and non-carriers

The fitted lines are based on all data points extending to -38 to +20. Left of EYO 0 is before expected symptom onset, and right of EYO 0 is after expected symptom onset. The EYO were first jittered, and then the data points before -20 and after EYO +8 removed to avoid accidental unblinding of participants. Dotted line is the point of divergence between mutation carriers and non-carriers. N=439.

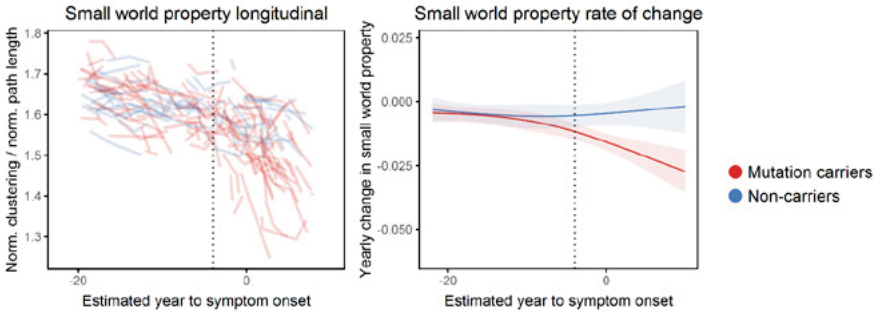

Figure 2 Rate of change grey matter network for mutation carriers and non-carriers by estimated year of onset

The fitted lines are based on all data points extending to -38 to +20. Left of EYO 0 is before expected symptom onset, and right of EYO 0 is after expected symptom onset. The EYO were first jittered, and then the data points before -20 and after EYO +8 removed to avoid accidental unblinding of participants. Dotted line is the point of divergence between mutation carriers and non-carriers.

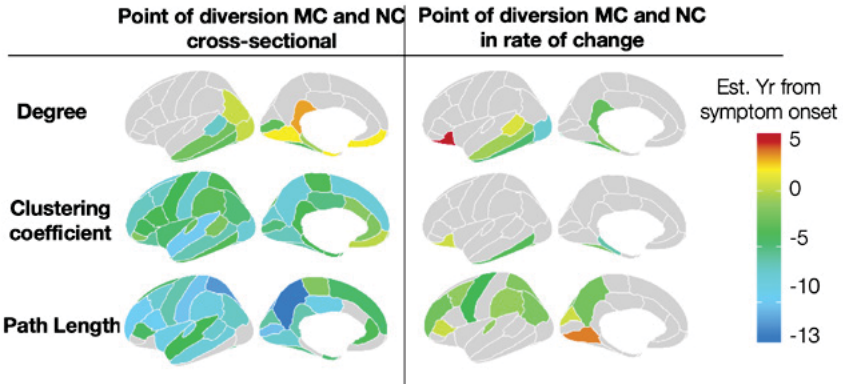

Figure 3 Regional EYO of diversion between mutation carriers and non-carriers for grey matter network degree, clustering coefficient and path length

Linear mixed models adjusted for sex, total grey matter volume and regional volume. MC=mutation carrier, NC= non-carrier. For details EYO by region see supplement table S3. N=416.

3.2 Longitudinal divergences between mutation carriers compared to non-carriers

When comparing rates of change over time, mutation carriers diverged from non-carriers by EYO for all grey matter network metrics, except connectivity density. Steeper decline for mutation carriers relative to non-carriers was detected earliest for network size, at baseline EYO -6.0, followed by small world coefficient at EYO -4.7, normalized clustering at EYO -4.6, degree at EYO -4.4, normalized path length at EYO -2.8, clustering coefficient at EYO -2.6, and path length at +1.0 (Figure 2, Sup.

Table S2 and Figure S1). When additionally adjusting for degree the estimates for network metrics yielded similar results, except for clustering coefficient, which lost significance. On a regional level, the earliest steep decline rate for mutation carriers compared to non-carriers was detected for degree in the lateral occipital gyrus at EYO -7.4, for clustering in the parahippocampal gyrus at EYO -6.2, and for path length in the precentral gyrus at EYO -4.2. (Figure 3, Supplement Table S3).

3.3 Association of grey matter networks with other neuroimaging and cognition

Established markers of Alzheimer disease showed significant relationships with the small world coefficient used as a global network summary statistic. We examined crossmodal relationships between baseline markers; over repeated measures; and whether baseline values could predict further decline in the other marker. We found that higher Aβ deposition load on PET was cross-sectionally related to a lower small world coefficient (β±SE = -0.22±0.05, p=3x10-6, Figure 4). In a longitudinal design, faster amyloid accumulation over time related to concurrent small world coefficient decline (β±SE = -0.33±0.06, p=1x10-7). Thirdly, a higher amyloid load at baseline predicted steeper decline of the small world coefficient over time (β±SE = -0.07±0.01, p=4x10-8).

Grey matter networks and the markers of Alzheimer disease progression showed significant relationships, both cross-sectionally and longitudinally (Figure 5). Specifically, a lower small world coefficient was cross-sectionally related to lower FDG-PET metabolism in the meta-ROI (B±SE = 0.44±0.08, p=2x10-7), as well as lower precuneus cortical thickness (β±SE = 0.50±0.06, p=2x10-15). For cognition, a lower small world coefficient was cross-sectionally related to lower scores on the DIAN

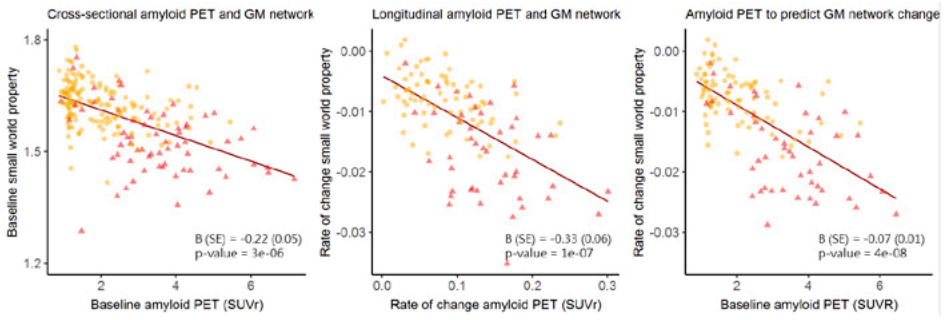

Figure 4 Association of amyloid PET with grey matter network small world coefficient in mutation carriers

For visualization purposes plotted extracted slopes with mixed model and line fitted with simple regression line in ggplot in R. Models to obtain beta and p-values specified in methods. GM network = grey matter network. Yellow circle = CDR 0 at baseline, Red triangle = CDR>0 at baseline. Amyloid PET = precuneus SUVr, Cross-sectional n= 222, Longitudinal n= 120, Predict change n= 131. For other grey matter network metrics see supplemental figure S2.

cognitive composite (β±SE = 0.28±0.08, p=3 x10-4). In a longitudinal design, decline of the small world coefficient over time related to concurrent decreases of FDG-PET metabolism (β±SE = 0.54±0.06, p=5x10-14) and faster precuneus cortical thinning (β±SE = 0.55±0.06, p=1 x10-17). A declining small world coefficient over time was related to concurrent decline on the cognitive composite (β±SE = 0.47±0.06, p=2x10-11). Thirdly, a lower small world coefficient at baseline predicted faster neurodegeneration as measured by FDG-PET metabolism (β±SE = 0.12±0.02, p=2x10-8) and precuneus cortical thinning (β±SE = 0.10±0.01, p=4x10-12), and steeper cognitive decline over time (composite B±SE = 0.08±0.02, p=2 x10-7). Associations for the other network properties can be found in Sup. Figures S2-5.

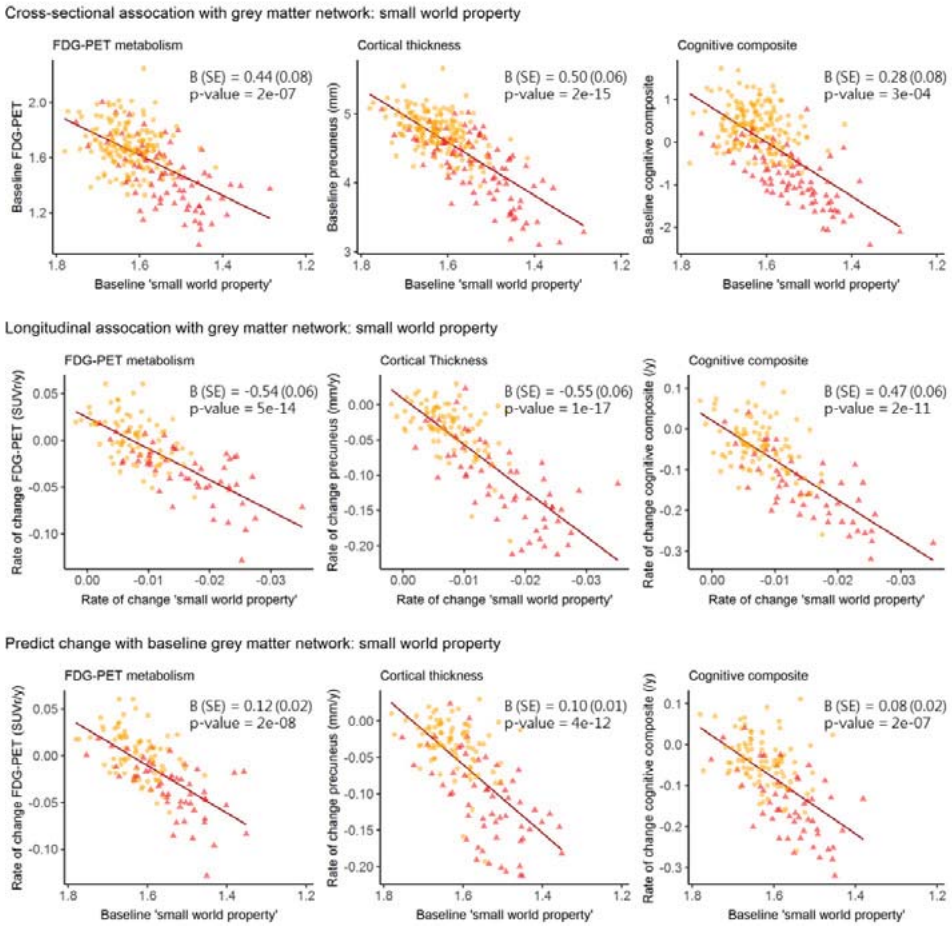

Figure 5 Associations of grey matter network small world coefficient with FDG-PET metabolism, cortical thickness and cognition

For visualization purposes plotted extracted slopes with mixed model and line fitted with simple regression line in ggplot in R. Models to obtain beta and p-values specified in methods. Inversed small world coefficient to aid visualization, see also supplemental table S4. Yellow circle = CDR 0 at baseline, Red triangle = CDR>0 at baseline. MRI thickness = cortical thickness precuneus, FDG-PET = METAROI SUVr as described in methods. DIAN composite: equally weighted z-score of Logical Memory Delayed Recall of the Wechsler memory test, DIAN Word List Test (comparable to International Shopping List Test), Digit Symbol Substitution Test and Mini Mental State Examination. Cross-sectional FDG-PET N=238 MR thickness n= 260, Cognition N=251; Longitudinal: FDG-PET n= 129 MR thickness n=146 , Cognition N= 140;Predict change: FDG-PET n= 131 MR thickness n= 146, Cognition n= 143. For other grey matter network metrics see supplemental figures S3-5.

4 Discussion

Using a single-subject approach, we found that structural grey matter networks deteriorate over the course of autosomal dominant Alzheimer disease and that moving to a more random topology closely correlates with cognitive function. When comparing mutation carriers to non-affected family members global network disruptions were detected cross-sectionally as early as 12 years before expected symptom onset. Longitudinally, increased rates of decline of network metrics were evident from 6 years before expected symptom onset. In line with our hypotheses based on cross-sectional studies in sporadic AD, grey matter network disruptions were associated with abnormalities and decline of established markers of Alzheimer disease. Thus, our grey matter network analysis in this unique cohort of autosomal dominant Alzheimer disease can contributes to our understanding of the Alzheimer disease trajectory, and indicates that our methods may potentially be a useful additional non-invasive tool for tracking disease progression. As Alzheimer disease progresses, there is substantial amyloid accumulation, volumetric loss, hypometabolism, and cognitive decline, but how grey matter networks fit into these processes remained unclear. Prior work in sporadic Alzheimer disease has shown that grey matter networks might be sensitive to biological changes during the preclinical stages of the disease [25-27]. In the current work, we observed similar alterations of grey matter networks in autosomal dominant Alzheimer disease as a function of estimated years to symptom onset. Using amyloid PET, we extended previous cross-sectional findings from studies in sporadic Alzheimer disease [26], by showing that higher baseline amyloid PET and higher amyloid accumulation rates are related to faster decline of grey matter networks over time. The consistency between sporadic and autosomal dominant Alzheimer disease strengthens the hypothesis that grey matter network disruptions are one of the downstream effects of amyloid accumulation. The networks were also related to sensitive markers of Alzheimer disease neurodegeneration and cognitive decline, in cross-sectional and longitudinal design. This suggested these processes occur, at least partly, in parallel [40], and supports the notion that grey matter network decline is a sign of progression of Alzheimer disease.

Previous studies in sporadic Alzheimer disease had suggested decline over time of grey matter networks, as there was a decrease over disease stages cross-sectionally [22, 27, 55]. Here, we show that grey matter networks decline over time

within individuals, and how decline rates start to increase with disease severity. Differences between mutation carriers and non-carriers in the rate of decline were generally detected later than cross-sectionally, which could have occurred because cross-sectional estimates across individuals by EYO may overestimate changes due to variance in the EYO measure (i.e., Some individuals at EYO -12 are actually only 5 or 6 years from actual onset) [35]. Another potential cause of cross-sectional and longitudinal estimate differences include sample sizes, with less individuals who had longitudinal data. Measurement variability over repeated measures within individuals can also have contributed to later detection of differences in the longitudinal design if these exceeded subtle rates of change. By extending follow-up time and numbers, an earlier observation decline over time may be possible.

Altering of network properties was not detected for every metric. This may be an indication that these metrics pick up different aspects of neurodegeneration. The small world measures (normalized clustering, and normalized path length and small world coefficient) showed early cross-sectional changes and seemed most sensitive to measure change over time. This is in line with network theory and previous findings in Alzheimer disease [23], which indicated that brain networks tend to become more similar to random networks over the disease course. The normalized network metrics reflect how different a network is from random, which may be why these best capture decline over time. Future studies should identify the most valid summary statistic to track longitudinal grey matter network disruptions.

On a regional level, cross-sectional network alterations were evident earliest in the parietal regions, and then spread across the brain. Most brain regions showed a difference first for path length, then for clustering and then for degree, except for the temporal regions, in which earlier and more pronounced lowering of the clustering coefficient was seen. Regional cross-sectional patterns showed early alterations for path length and clustering in areas with most pathology in autosomal dominant Alzheimer disease, including the precuneus. Regions of the default mode network also showed early alterations. Compared to previous sporadic Alzheimer disease studies, we find more widely affected connectivity, but the patterns are largely overlapping [23, 26, 56].

Compared to other structural grey matter imaging, the cross-sectional differences in the most sensitive grey matter network metrics were detected earlier than cortical thickness and volumetric measures. It was not part of this study to investigate whether grey matter networks have the same or higher sensitivity to early alterations than other structural MRI markers. Still, we adjusted for grey matter volume to assure measuring value beyond simple volumes. The rates of change were detected at a similar stage to the volumetrics, and later precuneus cortical thinning in dominantly inherited Alzheimer disease, which is the earliest region of change [36, 39]. The results merit application of grey matter networks in future deeper investigations, for example using multimodal network approaches with white matter and functional connectivity, to better understand the substrate of cognitive decline. The observation that network disruptions increase over time in a large multicenter study is relevant for clinical trials.

As the method only requires standard T1 scans and the available pipeline for network calculation, a next step is to test the approach retrospectively in clinical trial populations. One of the strengths of the current study design is the use of a previously validated method for grey matter network extraction. The unique traits of the DIAN cohort provided the ability to map changes in grey matter networks across decades of disease time. It should be noted that the estimates as a function of the expected symptom onset in dominantly inherited Alzheimer disease are influenced by sample size. Still, this method provides a way to detect and compare changes due to Alzheimer disease before symptom onset, and combine different families. Additionally, the rich characterization of DIAN participants provided the ability to relate observed changes in networks to other neuroimaging markers of pathology as well as cognition. A potential limitation is that our study included an average time period of 3 years in the longitudinal cohort, which may not be enough time to reliably measure changes due to Alzheimer disease in its very early stages. Yet, we show the longitudinal analysis of structural grey matter networks alongside of the cross-sectional results, which to the best of our knowledge has not been studied before and warrants further investigation of how grey matter networks deteriorate over time in sporadic Alzheimer disease.

In conclusion, in autosomal dominant Alzheimer disease individual grey matter networks are robustly associated with Alzheimer disease severity and progression as shown by the associations with EYO, amyloid accumulation, rate of neurodegeneration, and cognitive decline. These data suggest that single-subject grey matter networks obtained from structural MRI scans provide an additional, non-invasive tool for understanding and measuring progression from preclinical to severe clinical stages of Alzheimer disease. These grey matter networks can reflect the asynchronous start of brain pathology following Alzheimer disease-related cellular damage and inflammatory processes, informing about changes in grey matter covariance [56].

Acknowledgements

The authors are thankful towards all research participants of the DIAN cohort and their families, as well as to all participating researchers and coordinators, and those involved in processing and sharing of the data of DIAN (https://dian.wustl.edu/our-research/observational-study/dian-observational-study-sites/). Data collection and sharing for this project was supported by The Dominantly Inherited Alzheimer's Network (DIAN, UF1AG032438) funded by the National Institute on Aging (NIA), the German Center for Neurodegenerative Diseases (DZNE), Raul Carrea Institute for Neurological Research (FLENI), Partial support by the Research and Development Grants for Dementia from Japan Agency for Medical Research and Development, AMED (17929884, 16815631), and the Korea Health Technology R&D Project through the Korea Health Industry Development Institute (KHIDI).This manuscript has been reviewed by DIAN Study investigators for scientific content and consistency of data interpretation with previous DIAN Study publications.

Declarations

Funding: Alzheimer Nederland Fellowship 2018 (L.V.), ZonMW Memorabel grant #73305056 (B.M.T.) and #733050824 (B.M.T. and P.J.V.). IMI-JU n115736, European Union's Seventh Framework Programme (FP7/2007–2013), EFPIA companies' in kind contribution (L.V., P.J.V., P.S.). Willman Scholar Fund of the Barnes Jewish Hospital Foundation K01 AG053474 (B.A.G). Data collection and sharing for this project was supported by DIAN (grant no. UF1AG032438) funded by the National Institute on Aging and the German Center for Neurodegenerative Diseases (DZNE). Additional support came from the National Institutes of Health-funded NINDS Center Core for Brain Imaging (grant no. P30NS098577), the National Science Foundation (grant no. DGE-1745038), National Institutes of Health (grant no. UL1TR001873 to J.M.N.), the Swiss National Science Foundation (grant no. 320030-160221 to J.K.), the National Institute for Health Research University College London Hospitals Biomedical Research Centre, and the MRC Dementias Platform UK (grant nos. MR/L023784/1 and MR/009076/1). Computations were performed using the facilities of the Washington University Center for High Performance Computing, which were partially funded by NIH grants 1S10RR022984–01A1 and 1S10OD018091–01.

Competing interests: C.C. receives research support from Biogen, EISAI, Alector and Parabon, and is a member of the advisory board of ADx Healthcare, Halia Terapeutics and Vivid Genomics. N. G-R. reports taking part in multicenter studies funded by Biogen, Novartis, AbbVie and Eli Lilly. J.J.H. serves as a paid consultant and/or Advisory Board member for Biogen, Takeda, Lundbeck, Eisai, and Parabon. J.L. reports speaker's fees from Bayer Vital, speaker's fees from Willi Gross Foundation, consulting fees from Axon Neuroscience, consulting fees from Ionis Pharmaceuticals, non-financial support from Abbvie, outside the submitted work. E.mcD reports (research Funding); Eli Lilly- DSMB; ESAI - CMS; Alzamend - scientific advisory board. P.S. has acquired grant support (for the institution) from GE Healthcare, Danone Research, Piramal, and Merck. In the past 2 years, he has received consultancy/ speaker fees (paid to the institution) from Lilly, GE Healthcare, Novartis, Sanofi, Nutricia, Probiodrug, Biogen, Roche, Avraham, and EIP Pharma. Outside of this manuscript, R.J.B. reports grant/research/clinical trial support: NIH, Alzheimer's Association, BrightFocus Foundation, Rainwater Foundation Tau Consortium, Association for Frontotemporal Degeneration, Cure Alzheimer's Fund, the Tau SILK Consortium (AbbVie, Biogen, and Eli Lilly), Janssen, and an anonymous foundation. R.J.B. reports consulting fees/honoraria from Janssen, Pfizer, Roche, Eisai, and Merck. R.J.B. reports equity ownership interest/advisory board income from C2N Diagnostics. All other authors report no disclosures.

References

1. Scheltens, P., et al., Alzheimer's disease. Lancet, 2016. 388(10043): p. 505-17.
2. Aisen, P., et al., EU/US/CTAD Task Force: Lessons Learned from Recent and Current Alzheimer's Prevention Trials. J Prev Alzheimers Dis, 2017. 4(2): p. 116-124.
3. Jack, C.R., Jr., et al., NIA-AA Research Framework: Toward a biological definition of Alzheimer's disease. Alzheimers Dement, 2018. 14(4): p. 535-562.
4. Franzmeier, N., et al., Left frontal hub connectivity delays cognitive impairment in autosomal-dominant and sporadic Alzheimer's disease. Brain, 2018. 141: p. 1186-1200.
5. Chhatwal, J.P., et al., Preferential degradation of cognitive networks differentiates Alzheimer's disease from ageing. Brain, 2018. 141(5): p. 1486-1500.
6. Bassett, D.S. and E.T. Bullmore, Human brain networks in health and disease. Curr Opin Neurol, 2009. 22(4): p. 340-7.
7. Tijms, B.M., et al., Similarity-based extraction of individual networks from gray matter MRI scans. Cereb Cortex, 2012. 22(7): p. 1530-41.
8. Li, Y., et al., Discriminant analysis of longitudinal cortical thickness changes in Alzheimer's disease using dynamic and network features. Neurobiol Aging, 2012. 33(2): p. 427 e15-30.
9. He, Y., Z. Chen, and A. Evans, Structural insights into aberrant topological patterns of large-scale cortical networks in Alzheimer's disease. J Neurosci, 2008. 28(18): p. 4756-66.
10. Alexander-Bloch, A., J.N. Giedd, and E. Bullmore, Imaging structural co-variance between human brain regions. Nat Rev Neurosci, 2013. 14(5): p. 322-36.
11. Alexander-Bloch, A., et al., The convergence of maturational change and structural covariance in human cortical networks. J Neurosci, 2013. 33(7): p. 2889-99.
12. Zielinski, B.A., et al., Network-level structural covariance in the developing brain. Proc Natl Acad Sci U S A, 2010. 107(42): p. 18191-6.
13. Mechelli, A., et al., Structural covariance in the human cortex. J Neurosci, 2005. 25(36): p. 8303-10.
14. Seeley, W.W., et al., Neurodegenerative diseases target large-scale human brain networks. Neuron, 2009. 62(1): p. 42-52.
15. Draganski, B., et al., Neuroplasticity: changes in grey matter induced by training. Nature, 2004. 427(6972): p. 311-2.
16. Seidlitz, J., et al., Morphometric Similarity Networks Detect Microscale Cortical Organization and Predict Inter-Individual Cognitive Variation. Neuron, 2018. 97(1): p. 231-247 e7.
17. Doucet, G.E., et al., Person-Based Brain Morphometric Similarity is Heritable and Correlates With Biological Features. Cereb Cortex, 2019. 29(2): p. 852-862.
18. He, Y., Z.J. Chen, and A.C. Evans, Small-world anatomical networks in the human brain revealed by cortical thickness from MRI. Cereb Cortex, 2007. 17(10): p. 2407-19.
19. Humphries, M.D. and K. Gurney, Network 'small-world-ness': a quantitative method for determining canonical network equivalence. PLoS One, 2008. 3(4): p. e0002051.
20. Kim, H.J., et al., Using Individualized Brain Network for Analyzing Structural Covariance of the Cerebral Cortex in Alzheimer's Patients. Front Neurosci, 2016. 10: p. 394.
21. Tijms, B.M., et al., Single-subject grey matter graphs in Alzheimer's disease. PLoS One, 2013. 8(3): p. e58921.
22. Yao, Z., et al., Abnormal cortical networks in mild cognitive impairment and Alzheimer's disease. PLoS Comput Biol, 2010. 6(11): p. e1001006.
23. Tijms, B.M., et al., Gray matter networks and clinical progression in subjects with predementia Alzheimer's disease. Neurobiol Aging, 2018. 61: p. 75-81.
24. Dicks, E., et al., Gray matter network measures are associated with cognitive decline in mild cognitive impairment. Neurobiol Aging, 2018. 61: p. 198-206.
25. Tijms, B.M., et al., Gray matter network disruptions and amyloid beta in cognitively normal adults. Neurobiol Aging, 2016. 37: p. 154-160.

26. Ten Kate, M., et al., Gray Matter Network Disruptions and Regional Amyloid Beta in Cognitively Normal Adults. Front Aging Neurosci, 2018. 10: p. 67.
27. Voevodskaya, O., et al., Altered structural network organization in cognitively normal individuals with amyloid pathology. Neurobiol Aging, 2018. 64: p. 15-24.
28. Villemagne, V.L., et al., Amyloid beta deposition, neurodegeneration, and cognitive decline in sporadic Alzheimer's disease: a prospective cohort study. Lancet Neurol, 2013. 12.
29. Donohue, M.C., et al., Estimating long-term multivariate progression from short-term data. Alzheimers Dement, 2014. 10(5 Suppl): p. S400-10.
30. Young, A.L., et al., A data-driven model of biomarker changes in sporadic Alzheimer's disease. Brain, 2014. 137(Pt 9): p. 2564-77.
31. Roe, C.M., et al., Incident cognitive impairment: longitudinal changes in molecular, structural and cognitive biomarkers. Brain, 2018. 141(11): p. 3233-3248.
32. Vermunt, L., et al., Duration of preclinical, prodromal, and dementia stages of Alzheimer's disease in relation to age, sex, and *APOE* genotype. Alzheimers Dement, 2019.
33. Bateman, R.J., et al., Clinical and biomarker changes in dominantly inherited Alzheimer's disease. N Engl J Med, 2012. 367.
34. Ryman, D.C., et al., Symptom onset in autosomal dominant Alzheimer disease: a systematic review and meta-analysis. Neurology, 2014. 83(3): p. 253-60.
35. McDade, E., et al., Longitudinal cognitive and biomarker changes in dominantly inherited Alzheimer disease. Neurology, 2018. 91(14): p. e1295-e1306.
36. Gordon, B.A., et al., Spatial patterns of neuroimaging biomarker change in individuals from families with autosomal dominant Alzheimer's disease: a longitudinal study. Lancet Neurol, 2018. 17(3): p. 241-250.
37. Oxtoby, N.P., et al., Data-driven models of dominantly-inherited Alzheimer's disease progression. Brain, 2018. 141(5): p. 1529-1544.
38. Benzinger, T.L., et al., Regional variability of imaging biomarkers in autosomal dominant Alzheimer's disease. Proc Natl Acad Sci U S A, 2013. 110(47): p. E4502-9.
39. Kinnunen, K.M., et al., Presymptomatic atrophy in autosomal dominant Alzheimer's disease: A serial magnetic resonance imaging study. Alzheimers Dement, 2018. 14(1): p. 43-53.
40. Wang, G., et al., Staging biomarkers in preclinical autosomal dominant Alzheimer's disease by estimated years to symptom onset. Alzheimers Dement, 2019. 15(4): p. 506-514.
41. Morris, J.C., The Clinical Dementia Rating (CDR): current version and scoring rules. Neurology, 1993. 43(11): p. 2412-4.
42. Bateman, R.J., et al., The DIAN-TU Next Generation Alzheimer's prevention trial: Adaptive design and disease progression model. Alzheimers Dement, 2017. 13(1): p. 8-19.
43. Jack, C.R., Jr., et al., Update on the magnetic resonance imaging core of the Alzheimer's disease neuroimaging initiative. Alzheimers Dement, 2010. 6(3): p. 212-20.
44. Rubinov, M. and O. Sporns, Complex network measures of brain connectivity: uses and interpretations. Neuroimage, 2010. 52(3): p. 1059-69.
45. Desikan, R.S., et al., An automated labeling system for subdividing the human cerebral cortex on MRI scans into gyral based regions of interest. Neuroimage, 2006. 31(3): p. 968-980.
46. Fischl, B., FreeSurfer. Neuroimage, 2012. 62(2): p. 774-781.
47. Maslov, S. and K. Sneppen, Specificity and stability in topology of protein networks. Science, 2002. 296(5569): p. 910-3.
48. Su, Y., et al., Quantitative Analysis of PiB-PET with FreeSurfer ROIs. Plos One, 2013. 8(11).
49. Su, Y., et al., Partial volume correction in quantitative amyloid imaging. Neuroimage, 2015. 107: p. 55-64.

50. Landau, S.M., et al., Associations between cognitive, functional, and FDG-PET measures of decline in AD and MCI. Neurobiol Aging, 2011. 32(7): p. 1207-18.
51. Mishra, S., et al., Longitudinal brain imaging in preclinical Alzheimer disease: impact of *APOE* epsilon4 genotype. Brain, 2018. 141(6): p. 1828-1839.
52. Gelman, A., D. Lee, and J.Q. Guo, Stan: A Probabilistic Programming Language for Bayesian Inference and Optimization. Journal of Educational and Behavioral Statistics, 2015. 40(5): p. 530-543.
53. Carpenter, B., et al., Stan: A Probabilistic Programming Language. Journal of Statistical Software, 2017. 76(1): p. 1-29.
54. Bates, D., Maechler, M., Bolker, B., Walker, S. . lme4: Linear mixed-effects models using Eigen and S4. 2014; Available from: http://CRAN.R-project.org/package=lme4.
55. Tijms, B.M., et al., Alzheimer's disease: connecting findings from graph theoretical studies of brain networks. Neurobiol Aging, 2013. 34(8): p. 2023-36.
56. Verfaillie, S.C.J., et al., A more randomly organized grey matter network is associated with deteriorating language and global cognition in individuals with subjective cognitive decline. Hum Brain Mapp, 2018. 39(8): p. 3143-3151.

Supplemental data Chapter 4.1

Table S1 Summary data other modalities

		Asymptomatic mutation carriers (N=174)	Symptomatic mutation carriers (N=95)
N observations per participant	Amyloid PET scans, 1/2/3/4-7	83/ 58/ 16/ 3	31/ 28/ 11/ 6
	FDG-PET scans, 1/2/3/4-7	88/ 54/ 21/ 3	28/ 33/ 11/ 9
	Cognitive composite, 1/2/3/4-7	76/ 61/ 27/ 5	33/ 22/ 12/ 16
Baseline value	Amyloid PET precuneus, SUVr	2.0 (1.0)	3.5 (1.4)
	FDG-PET, DIAN METAROI	1.68 (0.16)	1.46 (0.23)
	Cognitive composite, z-score	0.37 (0.50)	-0.83 (0.64)
	Cortical thickness precuneus	4.8 (0.3)	4.2 (0.5)
	Total grey matter volume*1000	627 (64)	567 (72)

Mean (SD), unless otherwise specified. DIAN METAROI = Mean of 4 Desikan regions of Freesurfer: isthmus cingulate and inferior parietal, both left and right hemisphere. DIAN composite: equally weighted z-score of Logical Memory Delayed Recall of the Wechsler memory test, DIAN Word List Test (comparable to International Shopping List Test), Digit Symbol Coding and Mini Mental State Examination.

Table S2 Divergence between carriers and non-carriers by estimated years to symptom onset (EYO) cross-sectional and longitudinal, with sensitivity analysis for different models

		EYO of divergence			
	Covariates: sex 0 = male - gm volume mean-centered	Covariates: - sex 0 = female - gm volume mean-centered	Covariates: - sex 0 = male - gm volume mean-centered - average degree mean-centered	No covariates. with family term	No covariates. no family term
	Cross-sectional				
Size	no diff	no diff	n/a	no diff	
Average degree	0.0	+1.0	n/a	-1.2	
Connectivity Density	-5.6	-5.6	n/a	-5.8	
Average clustering	-7.5	-7.3	-8.6	-7.6	
Normalized clustering	-8.7	-8.5	-9.6	-7.7	
Average path length	no diff	no diff	n/a	-3.5	
Normalized path length	-12	-11.9	-12.4	-8.8	
Small world property	-8.4	-8	-7.7	-7.5	
	Longitudinal				
Size	-6.0	-6.3	n/a	-6.1	-6.0
Average degree	-4.4	-4.0	n/a	-3.4	-3.5
Connectivity Density	no diff	no diff	n/a	no diff	no diff
Average clustering	-2.6	-3.3	no diff	-3.5	-2.8
Normalized clustering	-4.6	-4.4	-4.5	-4.7	-4.7
Average path length	+1.0	+0.9	-4.8	+1.1	+1.2
Normalized path length	-2.8	-3.0	-4.2	-2.4	-2.4
Small world property	-4.7	-4.7	-4.4	-4.3	-4.4

Output cross-sectional analysis 99% credible intervals of the difference line; gm volume = total grey matter volume; gm volume and average degree were mean-centered; all models include a random family intercept and in the longitudinal models also for subject intercept and slope.

Table S3 Regional point of divergence between carriers and non-carriers by estimated years to symptom onset (EYO) cross-sectionally and longitudinal rate of change

Lobe	Region	Cross-sectionally			Longitudinal rate of change		
		Degree	Clustering	Path length	Degree	Clustering	Path length
F/P/T	Insula	-	-4.7	-8.7	-	-	-
F	Caudal middle frontal	-	-6.8	-7.4	-	-	-1.1
F	Frontal pole	-	-0.8	-	-	-	-
F	Lateral orbitofrontal	-	-5.8	-	+4.7	+0.5	-
F	Medial orbito frontal	+1.7	+0.0	-	-	-	-
F	Para central	-	-3.8	-1.7	-	-	-
F	Pars opercularis	-	-4.0	-9.5	-	-	-
F	Pars orbitalis	-	-1.7	-	-	-	-
F	Pars triangularis	-	-4.3	-4.5	-	-	+0.4
F	Pre central	-	-4.2	-6.3	-	-	-4.2
F	Rostral middle frontal	-	-6.8	-9.7	-	-	-2.4
F	Superior frontal	-	-7.9	-4.6	-	-	-
F (C)	Caudal anterior cingulate	-	-1.4	-	-	-	-
F (C)	Rostral anterior cingulate	-	-1.8	-3.8	-	-	-
P	Inferior parietal	+0.4	-4.9	-6.9	-	-	-1.9
P	Post central	-	-7.4	-10.3	-	-	-
P	Precuneus	-	-7.9	-13.1	-	-	-2.3
P	Superior parietal	-	-3.8	-12.0	-	-	-1.7
P	Supramarginal	-	-3.3	-8.4	-	-	-1.0
P (C)	Isthmus cingulate	+3.0	-4.0	-6.3	-3.0	-	-
P (C)	Posterior cingulate	-	-5.2	-8.8	-	-	-
O	Cuneus	-	-7.4	-6	-	-	+0.5
O	Lateral occipital	+0.3	-7.6	-	-7.4	-	-
O	Lingual	+1.7	-6.7	-7.3	-	-	+3.5
O	Pericalcarine	-3.2	-5.0	-10.5	-	-	-
T	Banks superior temporal	-7.0	-2.0	-7.2	0.9	-	-
T	Entorhinal	+1.8	-4.1	-4.7	-	-	-
T	Fusiform	-3.5	-6.1	-5.3	-4	-2.1	-
T	Inferior temporal	-3.1	-3.7	-	-4.7	-3.6	-
T	Middle temporal	-2.4	-6.4	-7.9	-0.7	-	-
T	Parahippocampal	-0.7	-4.0	-	-1.4	-6.2	-
T	Superior temporal	-	-10.0	-4.2	-	-	-
T	Temporal pole	-	-4.2	-	-	-	-
T	Transverse temporal	-	-2.9	-8.4	-	-	-1.1

Output cross-sectional analysis 99% credible intervals of the difference line; all models include a random family intercept and in the longitudinal models also for subject intercept and slope. The models for degree are adjusted for baseline grey matter volume, mean-centered, baseline regional volume, mean-centered, and sex (0=male), and for clustering and path length also for baseline degree, mean-centered. T=temporal lobe, P=parietal lobe, F=frontal lobe, C=cingulate, O=occipital. EYO = estimated years to symptom onset.

Table S4 Associations between grey matter network small world property and other imaging and clinical markers in mutation carriers

Model	Outcome	Predictor	Beta (SE)	p-value
Model 1 Cross-sectional	Small world property	Amyloid PET	-0.22 (0.05)	3e-06
	FDG-PET	Small world property	0.44 (0.08)	2e-07
	MR thickness	Small world property	0.50 (0.06)	2e-15
	Cognitive composite	Small world property	0.28 (0.08)	3e-04
Model 2 Longitudinal; fixed effect predictor	Small world property	Amyloid PET	-0.33 (0.06)	1e-07
	FDG-PET	Small world property	0.54 (0.06)	5e-14
	MR thickness	Small world property	0.55 (0.06)	1e-17
	Cognitive composite	Small world property	0.47 (0.06)	2e-11
Model 3 Predict change with baseline value; fixed effect interaction predictor over time after baseline	Small world property	Amyloid PET	-0.07 (0.01)	4e-08
	FDG-PET	Small world property	0.12 (0.02)	2e-08
	MR thickness	Small world property	0.10 (0.01)	4e-12
	Cognitive composite	Small world property	0.08 (0.02)	2e-07

Linear models adjusted for baseline age, sex, total grey matter volume, and if possible family cluster. Additionally, in model 2 random effect for subject intercept and subject predictor slope, and in model 3 subject intercept and slope after baseline, plus fixed effect time after baseline and interaction between time and predictor. Amyloid PET = precuneus SUVr, MR thickness = cortical thickness precuneus, FDG-PET = METAROI SUVr as described in methods. DIAN composite: equally weighted z-score of Logical Memory Delayed Recall of the Wechsler memory test, DIAN Word List Test (comparable to International Shopping List Test), Digit Symbol Coding and Mini Mental State Examination. All predictor and outcome variables were scaled.

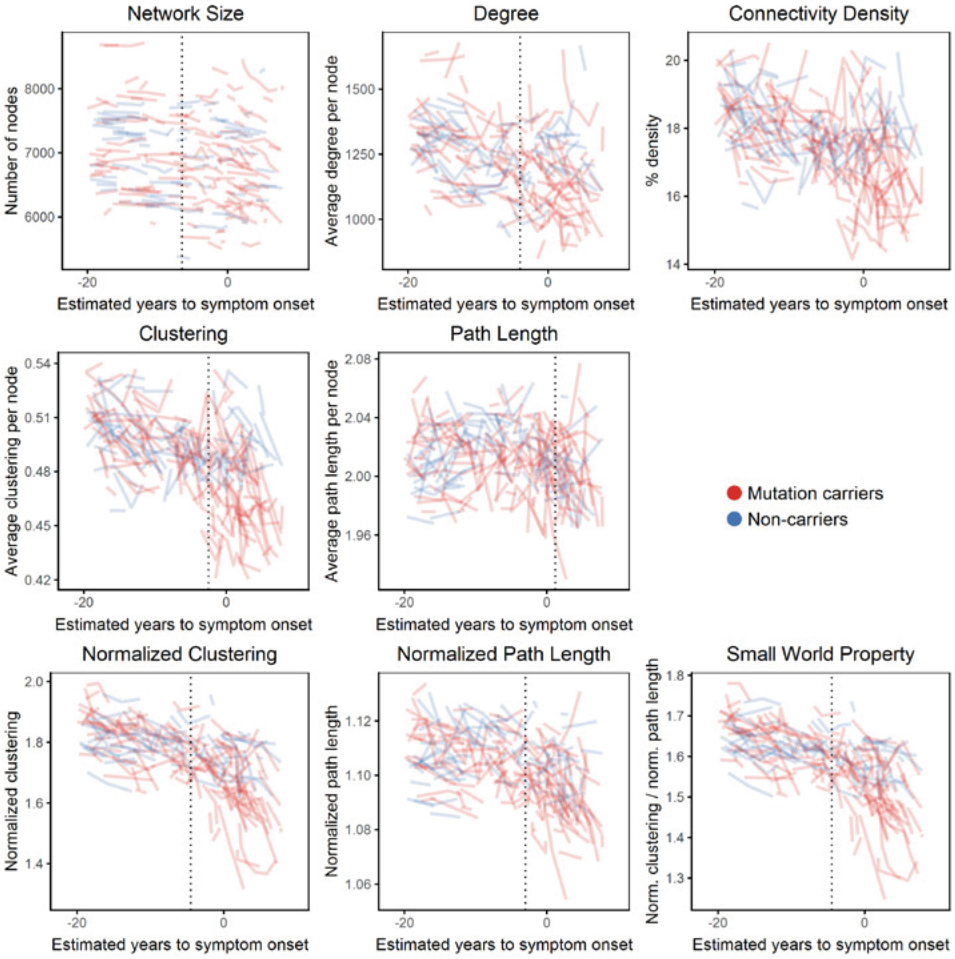

Figure S1 Raw data longitudinal grey matter networks with estimated points of divergence between mutation carriers and noncarriers

The fitted lines are based on all data points extending to -38 to +20. The graph was adapted to avoid accidental unblinding of participants, including 1 outlier removed. Left of EYO 0 is before expected symptom onset, and right of EYO 0 is after expected symptom onset. The EYO were first jittered, and then the data points before -20 and after EYO +8 removed. Dotted line is approximately the point of divergence between mutation carriers and non-carriers.

Parameters in statistical models

1 EYO comparisons:

a. Cross-sectional

$$\text{Network}_{\text{metric}} = \beta0 + \beta1*\text{EYO}_{\text{linear}} + \beta2*\text{EYO}_{\text{cubic}} + \beta3*\text{Mutation}_{\text{status}} + \beta4 * \text{EYO}_{\text{linear}}*\text{Mutation}_{\text{status}} + \beta5*\text{EYO}_{\text{cubic}}*\text{Mutation}_{\text{status}} + (\text{Random intercept}|\text{Family}_{\text{cluster}}) + \beta x*\text{covariates}$$

b. Longitudinal

$$\text{Network}_{\text{metric}} = \beta0 + \beta1*\text{EYO}_{\text{linear}} + \beta2*\text{EYO}_{\text{cubic}} + \beta3* \text{time} + \beta4\text{Mutation}_{\text{status}} + \beta5 * \text{EYO}_{\text{linear}}*\text{time} + \beta6*\text{EYO}_{\text{cubic}}*\text{time} + \beta7*\text{Mutation}_{\text{status}}* \text{time} + \beta8 * \text{EYO}_{\text{linear}}*\text{Mutation}_{\text{status}}* \text{time} + \beta9*\text{EYO}_{\text{cubic}}*\text{Mutation}_{\text{status}}*\text{time} + (\text{Random intercept+time }|\text{Individual}) + (\text{Random intercept}|\text{Family}_{\text{cluster}}) + \beta x*\text{covariates}$$

2 Crossmodal comparisons mutation carriers only

a. Cross-sectional

$$\text{Outcome}_{-\text{baseline}} = \beta0 + \beta1*\text{Predictor\_baseline} + (\text{Random intercept}|\text{Family}_{\text{cluster}}) + \beta x *\text{covariates}$$

b. Longitudinal

$$\text{Outcome} = \beta0 + \beta1*\text{Predictor} + (\text{Random intercept+predictor}|\text{Individual}) + (\text{Random intercept}|\text{Family\_cluster}) + \beta x*\text{covariates}$$

c. Predict rate of change over time

$$\text{Outcome} = \beta0 + \beta1*\text{Predictor}_{\text{baseline}} + \beta2*\text{time} + \beta3*\text{predictor}_{\text{baseline}}*\text{time} + (\text{Random intercept+time}|\text{Individual}) + (\text{Random intercept}|\text{Family}_{\text{cluster}}) + \beta x*\text{covariates}$$

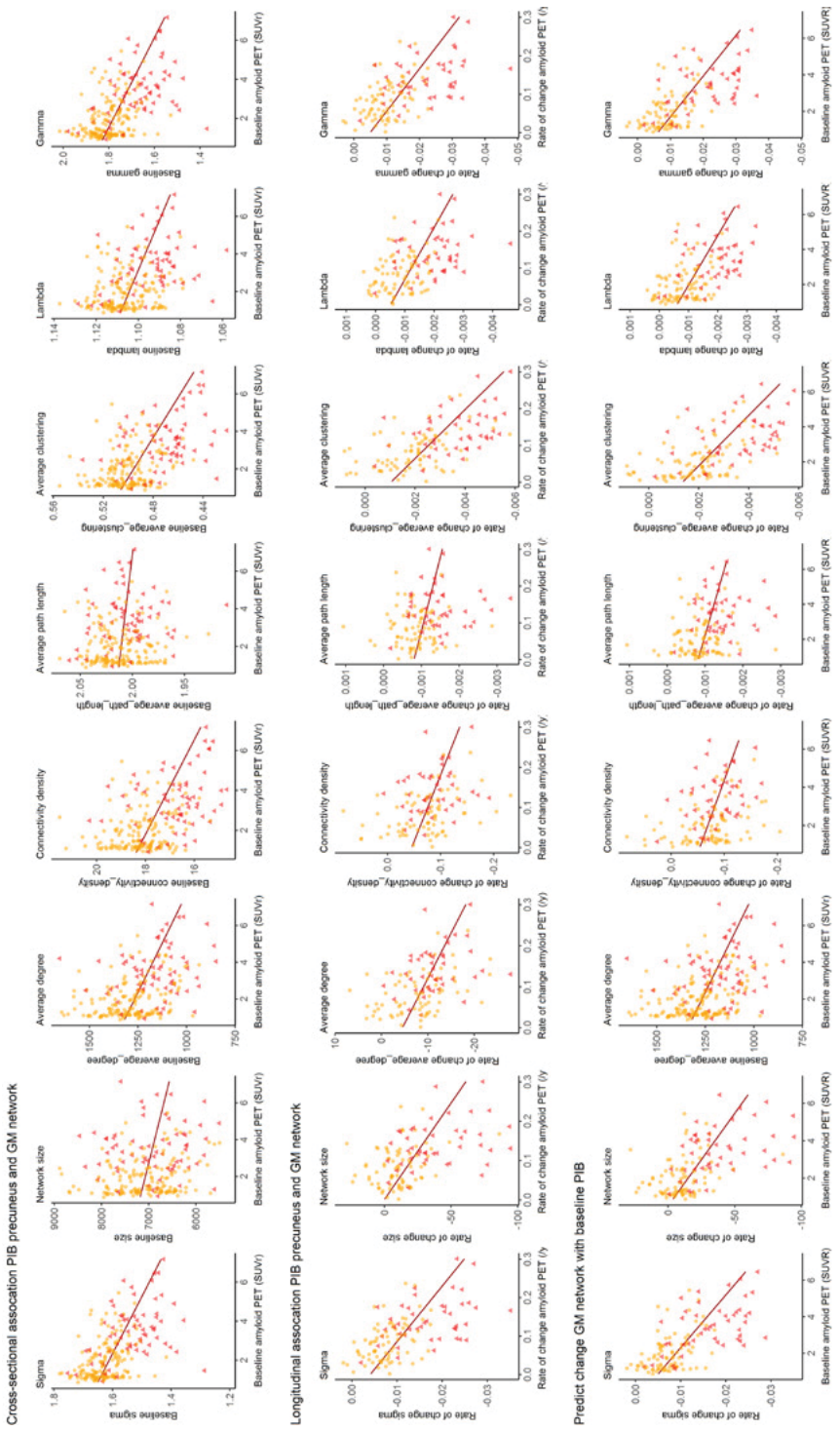

Figure S2 Comparisons PIB and other grey matter network with mutation carriers
Yellow circle = asymptomatic; red triangle = symptomatic at baseline

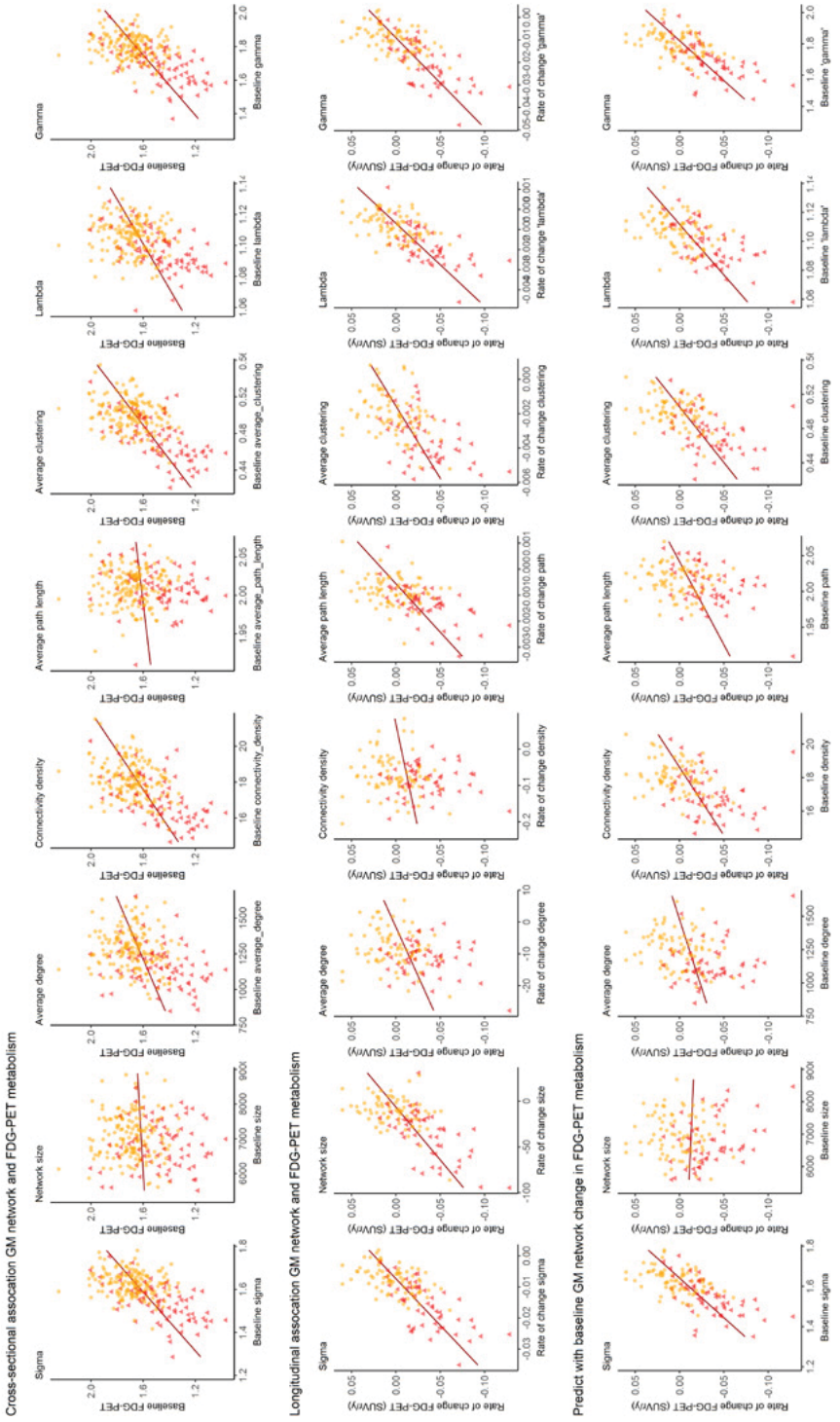

Figure S3 Comparisons other grey matter network measures and FDG metabolism in mutation carriers

Yellow circle = asymptomatic; red triangle = symptomatic at baseline

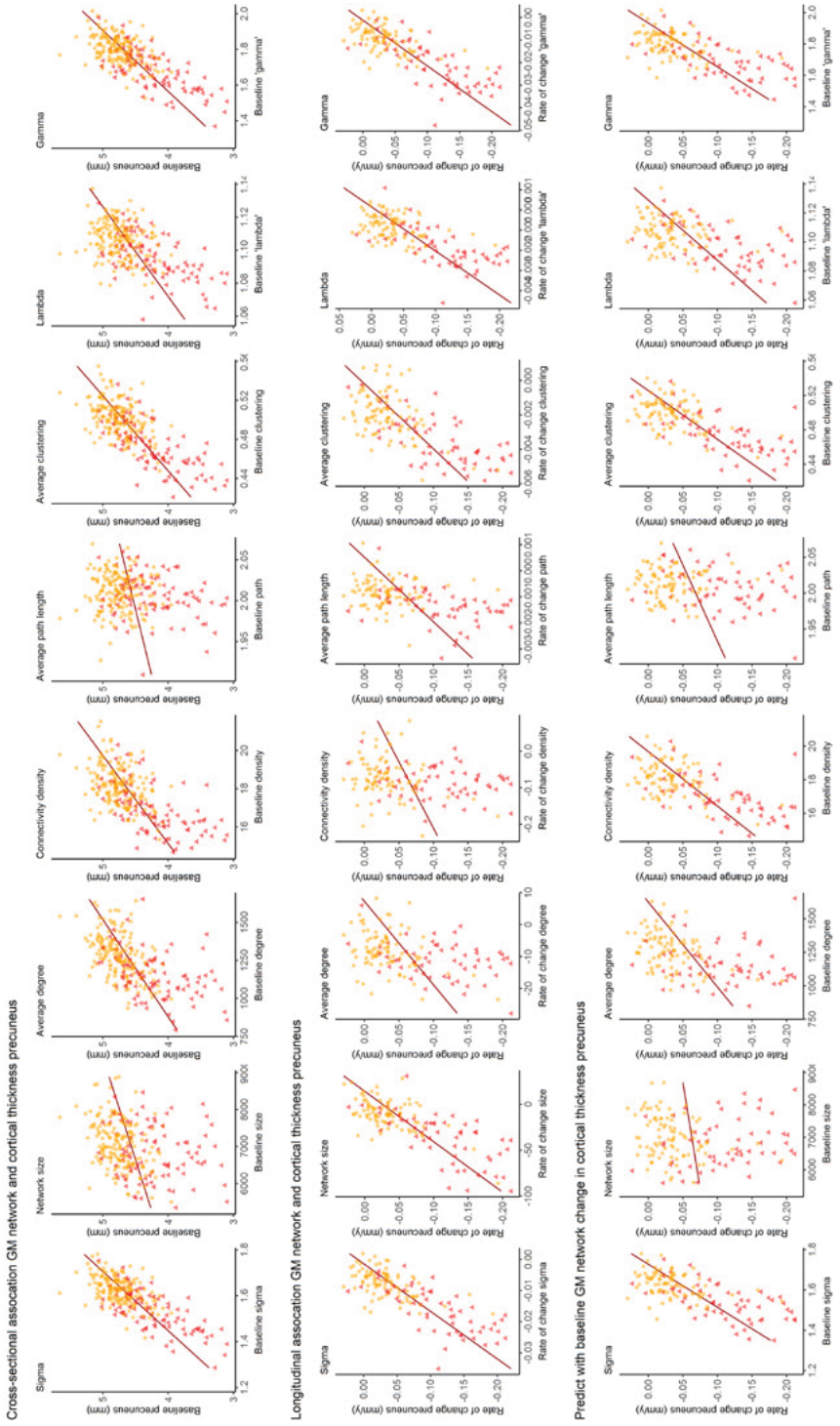

Figure S4 Comparisons other grey matter network measures and cortical thickness in mutation carriers

Yellow circle = asymptomatic; red triangle = symptomatic at baseline

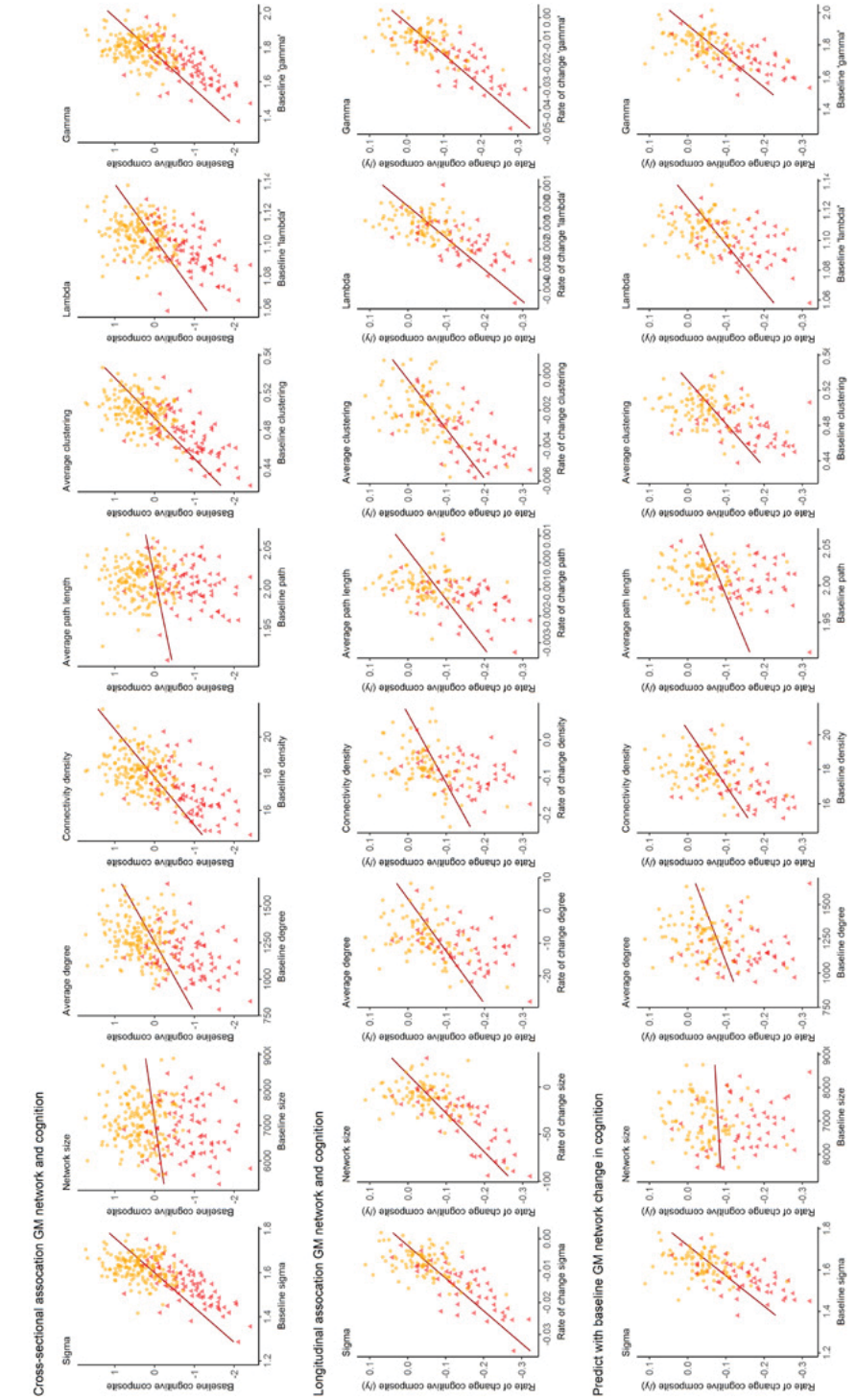

Figure S5 Comparisons other grey matter network measures and cognition in mutation carriers
Yellow circle = asymptomatic; red triangle = symptomatic at baseline

Chapter 4.2

Biological correlates of grey matter network disruption in autosomal dominant Alzheimer disease

Lisa Vermunt, Courtney Sutphen, Ellen Dicks, Sarah B. Berman, David M Cash, Jasmeer P. Chhatwal, Carlos Cruchaga, Michael Ewers, Nick Fox, Bernardino Ghetti, Neill R. Graff-Radford, Celeste Karch, Jens Kuhle, Christoph Laske, Johannes Levin, Colin L. Masters, E. McDade, Hiroshi Mori, John C. Morris, James M. Noble, Richard J. Perrin, Oliver Preische, Peter R. Schofield, Marc Suarez Calvet, Chengjie Xiong, Philip Scheltens, Pieter Jelle Visser, Tammie L.S. Benzinger, Randall J. Bateman, Anne M. Fagan, Brain A. Gordon, Betty M. Tijms, on behalf of DIAN investigators.

In preparation

Abstract

BACKGROUND: Structural grey matter covariance networks are disrupted in neurodegenerative disorders such as Alzheimer disease (AD). These disruptions are related to early amyloid aggregation and cognitive decline, but the precise biological underpinnings of network changes remain unknown. Besides amyloid aggregation, many other pathological processes occur in AD, including synaptic dysfunction and loss, axonal degeneration, neuronal damage, and inflammatory processes, that may contribute to grey matter network disruptions. Therefore, we investigated how cerebrospinal fluid (CSF) proteins concentrations, reflecting these pathological processes, are associated with grey matter network disruptions in autosomal dominantly inherited AD (ADAD) mutation carriers.

METHODS: From the Dominantly Inherited Alzheimer Network (DIAN) Observational study, we included 219 mutation carriers and 136 noncarriers with both T1-weighted MRI and CSF collection. CSF biomarkers included: $A\beta_{40/42}$ ratio (amyloid aggregation), pTau (hyperphosphorylation), tTau and VILIP-1 (neuronal injury and death), SNAP-25 and neurogranin, (synaptic damage), NfL (axonal injury), YKL-40 and soluble TREM2 (neuro-inflammation). We examined relationships between CSF levels of these markers and grey matter network integrity as quantified by the small world coefficient. This measure indicates whether networks deviate from a randomly organized network. We further tested whether relationships were dependent on disease stage, and fitted the trajectory of the disease course for each of the markers.

RESULTS: Increased pTau, tTau, SNAP-25, Ng, VILIP-1, NfL and YKL-40 were associated with lower small world values in mutation carriers. NfL showed the strongest relationship with the small world coefficient (β±SE = -0.72±0.05; p<0.001). Within carriers, these relationships were not significantly different across disease stages. Abnormalities in the traditional CSF biomarkers and synaptic and neuronal injury markers preceded grey matter network disruptions by several years, while YKL-40 and NfL abnormalities co-occurred.
CONCLUSION: Our results suggest that axonal loss may contribute to disrupted grey matter networks as observed in AD.

1 Introduction

Brain areas implicated in similar functions show covariation in cortical morphology on magnetic resonance imaging (MRI), and these covariation patterns can be precisely quantified with a network approach [1-3]. In neurodegenerative diseases, such as Alzheimer disease (AD), grey matter networks become disrupted [3-5]. With increasing disease severity in AD, grey matter networks become more randomly organized, as consistently indicated by a lower small world coefficient [6]. These network disruptions are related to impaired cognition and future cognitive decline, both in sporadic and autosomal dominant AD (ADAD) [6-13]. Network disruptions can already be detected in cognitively normal individuals with amyloid aggregation (presumed preclinical AD) [6, 14, 15]. Still, the biological mechanisms that explain the deterioration of network organization remain unclear. Changes in grey matter networks could result from multiple pathophysiological processes such as synaptic dysfunction and loss, axonal degeneration, neuronal loss, and local swelling in response to infiltration of inflammatory cells. A better understanding of network disruptions over the course of AD may inform new hypotheses regarding how brain connectivity could be maintained in order to preserve cognitive function.

In cerebrospinal fluid (CSF), proteins can be measured that reflect ongoing biological processes in the brain. CSF biomarkers are used for the biological definition of AD based on abnormal concentrations of β-amyloid 1-42 (ratio of β-amyloid 1-42/1-40 [$A\beta_{42/40}$]), hyperphosphorylation of tau (181-phosphorylated fraction [pTau]), and neuronal injury (total tau [tTau]) [16]. In addition to these core AD measures, other biomarkers have robustly been related to AD, and provide information on additional pathological brain alterations occurring in the disease [17]. Increased levels of synaptosomal-associated protein-25 (SNAP-25) and neurogranin (Ng) levels are markers of pre-synaptic and post-synaptic dysfunction, respectively; visinin-like protein 1 (VILIP-1) of neuronal death; and neurofilament light chain (NfL) of axonal damage [18-23]. In addition, chitinase-3-like protein 1 (YKL-40), an astrocyte marker, and soluble TREM2 (sTREM2) [19, 20, 23, 24], a marker of activated microglia, are also elevated in AD and provide insight into inflammatory processes. It is conceivable that abnormal of levels of these markers may impact brain connectivity, but this remains largely unknown.

Here, we studied this question in carriers of ADAD genetic mutations, which has the advantage of a relatively conserved dementia onset age and few age-related co-pathologies due to the relatively young age of symptoms [25]. We assessed the associations between both the core and emerging CSF biomarkers for AD and the individual grey matter network summary statistic the 'small world coefficient'. We further tested within mutation carriers whether the relationships observed were depended on disease stage, as determined by a combination of the pTau/$A\beta_{42}$ ratio (normal, abnormal) and the clinical dementia rating score (CDR).

2 Methods

2.1 Participants and design

Data was obtained from the Dominant Inherited Alzheimer Network Observational Study (DIAN-Obs) [26]. For the DIAN study, ADAD mutation carriers (MC) (presenilin 1 [PSEN1], presenilin 2 [PSEN2] and amyloid precursor protein [APP]) and their noncarrier (NC) family members undergo longitudinal clinical and cognitive examinations, neuroimaging and biospecimen donations. We evaluated data that passed quality control and was included in data freeze 12. Families with Flemish and Dutch mutations were excluded from analyses, because these mutation result in a different phenotype, with primarily cerebral amyloid angiopathy. The study was approved by the ethical review board at Washington University, St. Louis, Missouri, USA and local IRBs. The estimated years to symptom onset (EYO) for each individual was defined as the mutation-specific (e.g. for the PSEN1 G206A mutation, the mean age at onset is 53) mean age at onset subtracted from the individuals' visit age [25]. In case mutation age of onset was unknown, the family-specific parental age of disease onset was used instead. For example, if the mean age at symptom onset is 53 years for a specific family mutation, then a 43 year old individual, regardless of mutation status, would have an EYO of -10. This indicates an individual with the mutation is expected to show clinical symptoms of AD 10 years later, and allows comparison of biomarkers with the NCs on the same timeline, as well as between MCs and NCs from different families and mutations. For the for the biomarker comparisons, we selected the first visit at which individuals had both CSF and MRI data available.

2.2 Group definitions

Participants were stratified in two ways. The first set of analyses focus on comparing all MCs to their familial NC controls. The second set of analyses staged MCs into 4 groups based upon their biomarker status and CDR [27]. Group 1 had a normal CSF ratio of pTau/$A\beta_{42}$ (< 0.019 [28]) (indicating absence of underlying brain amyloid). Group 2-4 had abnormal ratios (indicating presence of amyloid) and increasing CDRs of: group 2: CDR= 0, no impairment; group 3: CDR = 0.5, very mild dementia; group 4: CDR >= 1 mild to severe dementia.

2.3 MR preprocessing

MR scans were collected and preprocessed according the protocols of the Alzheimer's Disease neuroimaging Initiative (1.1 by 1.1 by 1.2 mm^3 voxels, repetition time = 2300, echo time = 2.95, flip angle 9°), described in detail in [29, 30]. For the network extractions, T1-weighted scans were first segmented into grey matter, white matter and CSF in native space with Statistical Parametric Mapping 12 (SPM12; Wellcome Trust Centre for Neuroimaging, UCL Institute of Neurology, London, UK). The segmentations were checked and resliced into 2mm by 2mm by 2mm voxels, and this was the input for the grey matter network extraction.

2.4 Calculation of grey matter network metrics

Single-subject grey matter network metrics were extracted from preprocessed grey matter segmentations according to previously published procedures, (https://github.com/bettytijms/Single_Subject_Grey_Matter_Networks)[2] as follows: Grey matter segmentations were parcellated into cubes of 3 by 3 by 3 voxels, and these cubes formed the nodes of the network. The Pearson's correlation coefficient was then calculated for grey matter intensities across the voxels for each pair of cubes. Next, correlation values were binarized and only significant connections retained. Finally, we calculated for each network the small world coefficient using scripts from the brain connectivity toolbox (https://sites.google.com/site/bctnet/ [31] modified for large sized networks. In this study, we use the small world coefficient, which is a whole brain summary statistic and normalized for individual differences in degree and size of networks. A network with a small world coefficient of 1 has a random organization, while a value higher than 1 indicates the networks exhibits the 'small world property'. Technically, networks are 'small world' when the level of clustering is high, while the path length to every other node is still relatively short [32, 33].

2.5 Cerebrospinal fluid markers

Participants underwent lumbar puncture after overnight fasting. Samples were collected via gravity drip in polypropylene tubes and sent on dry ice to the DIAN biomarker laboratory at Washington University. The samples were aliquoted in 0.5mL polypropylene tubes, stored at -84°C before measurements of SNAP-25, Ng, VILIP-1 and YKL-40. Additional aliquots of each sample were shipped on dry ice for the measurements of $A\beta_{40}$, $A\beta_{42}$, pTau and tTau by the Shaw laboratory at the University of Pennsylvania [34], of NfL by the Kuhle laboratory in Basel [35], and of sTREM2 by the Haass laboratory in Münich [36]. For details on the protocols, see [21, 22, 24, 37]. Briefly, $A\beta_{40}$, $A\beta_{42}$, pTau and tTau levels were determined using the automated Elecsys assay, and values of $A\beta_{40}$ and $A\beta_{42}$ outside the measurement ranges were extrapolated on the calibration curve [37]. SNAP-25, Ng and VILIP-1 were measured with antibodies developed in the laboratory of Dr. Jack Ladenson at Washington University in St. Louis, as part of micro-particle-based immunoassays using the Singulex (now part of EMD Millipore; Alameda, CA) Erenna system [22]. YKL-40 was measured with

Table 1 Demographics and baseline summary data on predictors and outcomes.

	Noncarriers (NCs)		Mutation carriers (MCs)				
	All (n=136)	NCs < 40 years old (n=81)	All (n=216)	MCs: ratio neg (n=84)	MCs: CDR 0, ratio pos (n=63)	MCs: CDR 0.5, ratio pos (n=43)	MCs: CDR 1-3, ratio pos (n=26)
Demographics							
N (%) Male	53 (39%)	32 (40%)	96 (44%)	35 (42%)	28 (44%)	19 (44%)	14 (54%)
Age, years	38 ± 12	31 ± 6	39 ± 10	32 ± 8	38 ± 9	47 ± 9	47 ± 9
EYO, years	-10 ± 12	-17 ± 9	-9 ± 11	-17 ± 8	-8 ± 7	1 ± 6	4 ± 4
Years of education, median±IQR	15 ± 3	15 ± 2	14 ± 4	15 ± 3	15 ± 4	14 ± 4	12 ± 2
CDR (0/0.5-1/2-3), N	131/5/0	0/2/0	142/66/8	79/5/0	63/0/0	0/43/0	0/18/8
MMSE, median±IQR	30 ± 1	30 ± 1	29 ± 3	29 ± 1	29 ± 2	26 ± 4	16 ± 10
Grey matter network							
Small world coefficient	1.62 ± 0.05	1.65 ± 0.05	1.59 ± 0.08	1.64 ± 0.06	1.60 ± 0.05	1.55 ± 0.08	1.46 ± 0.07
Traditional CSF markers							
$A\beta_{42}$ pg/ml	1,407 ± 466	1,292 ± 442	974 ± 634	1,526 ± 655	716 ± 279	553 ± 208	510 ± 217
$A\beta_{40}$ pg/ml	15,698 ± 4418	14,398 ± 4,204	14,862 ± 4760	15,607 ± 5,080	15,004 ± 4,749	14,483 ± 4,114	12,741 ± 4,241
pTau pg/ml	14 ± 5	13 ± 4	31 ± 23	14 ± 4	32 ± 18	46 ± 23	57 ± 28
tTau pg/ml	169 ± 55	154 ± 49	290 ± 162	177 ± 48	305 ± 120	375 ± 142	475 ± 241
Ratio $a\beta_{42/40}$	0.089 ± 0.01	0.089 ± 0.007	0.066 ± 0.035	0.099 ± 0.031	0.049 ± 0.017	0.039 ± 0.012	0.042 ± 0.015
ratio $A\beta_{42/40}$ ↓0.075, N (%)	6 (4%)	1 (1%)	144 (67%)	19 (23%)	58 (92%)	42 (98%)	25 (96%)
ratio pTau/ $A\beta_{42}$	0.010 ± 0.004	0.010 ± 0.002	0.052 ± 0.053	0.010 ± 0.004	0.051 ± 0.034	0.091 ± 0.049	0.120 ± 0.065
ratio pTau/$A\beta_{42}$ ↑0.0198, N (%)	2 (1%)	0 (0%)	132 (61%)	-	-	-	-
Emerging CSF markers							
SNAP-25 pg/ml	3.6 ± 1.3	3.2 ± 1.1	4.6 ± 1.9	3.6 ± 1.1	4.5 ± 1.5	5.2 ± 1.7	6.4 ± 2.7
Ng pg/ml	1,563 ± 741	1,447 ± 765	2,297 ± 1,212	1,638 ± 682	2,526 ± 1,109	2,673 ± 1,164	3,120 ± 1,748
NfL pg/ml	793 ± 544	564 ± 396	1,939 ± 1,762	531 ± 190	1,033 ± 650	2,630 ± 1,643	3,873 ± 1,657
VILIP-1 pg/ml	133 ± 50	122 ± 48	174 ± 79	135 ± 47	179 ± 71	198 ± 75	236 ± 114
YKL-40 ng/ml	133 ± 66	98 ± 37	173 ± 88	109 ± 37	169 ± 69	229 ± 81	280 ± 89
sTREM2, relative to reference sample	0.47 ± 0.22	0.43 ± 0.21	0.58 ± 0.29	0.42 ± 0.15	0.48 ± 0.28	0.73 ± 0.3	0.74 ± 0.3

Legend: CSF biomarkers not available for the whole sample: SNAP (n=330), Ng (n=331), VILIP1 (n=330), YKL40 (n=331), NfL (n=169 (incl. 19 with no MRI data), sTREM2 (n=164).

plate-based enzyme-linked immunoassay (MicroVue ELISA; Quidel, San Diego, CA) [22]. NfL was measured with a single-molecule array assay using the capture monoclonal antibody 47:3 and biotinylated detection antibody 2:1 (UmanDiagnostics AB, Sweden) [21]. sTREM2 was measured using the MSD platform with an in-house developed ELISA based on commercially available antibodies [24]. The sTREM2 concentrations are reported relative to the pooled sample that was loaded onto all plate, as a way to account for plate variation.

2.6 Statistical analysis

In all linear models pTau, tTau, SNAP-25, Ng, VILIP-1, YKL-40, NfL and sTREM2 were log-transformed to approach normality. To aid comparability of slope estimates, the variables were Z-transformed according to the total group. We tested the associations between the CSF biomarkers as predictors and the small world coefficient as the outcome with three linear regression models. Model 1 was adjusted for sex; Model 2 also included a fixed term for mutation status and its interaction with the predictor; Model 3 had additional adjustment for age effects. We further performed a subgroup analysis within MCs only to investigate disease stage effects, by running models that included the CSF predictor, a fixed term for the severity groups and its interaction with the predictor. We ran post-hoc pairwise comparisons using the Tukey HSD procedure. Lastly, we estimated trajectories for all markers studied by EYO, using a previously developed Bayesian inference linear mixed effect model [29, 38] to obtain insight into the relative ordering of biomarker trajectories (details in Supplemental data). Before fitting this model, the CSF and MRI biomarkers were Z-scored to young NCs (<40 years old, n=81, table 1). All statistical analyses were conducted in R (version 3.5.3) using the stats, emmeans. car, lmer, rstan and stanarm-packages [39].

3 Results

The presented analyses included 136 NCs and 219 MCs (age mean±SD 39±11; EYO mean±SD -9±11). In the MC group, 84 (39%) individuals had normal CSF ratio pTau/$A\beta_{42}$. Among MCs with an abnormal CSF pTau/$A\beta_{42}$ ratio, 64 (29%) individuals had CDR 0, 43 (20%) CDR 0.5 and 26 (12%) CDR 1-3. The group characteristics are shown in Table 1.

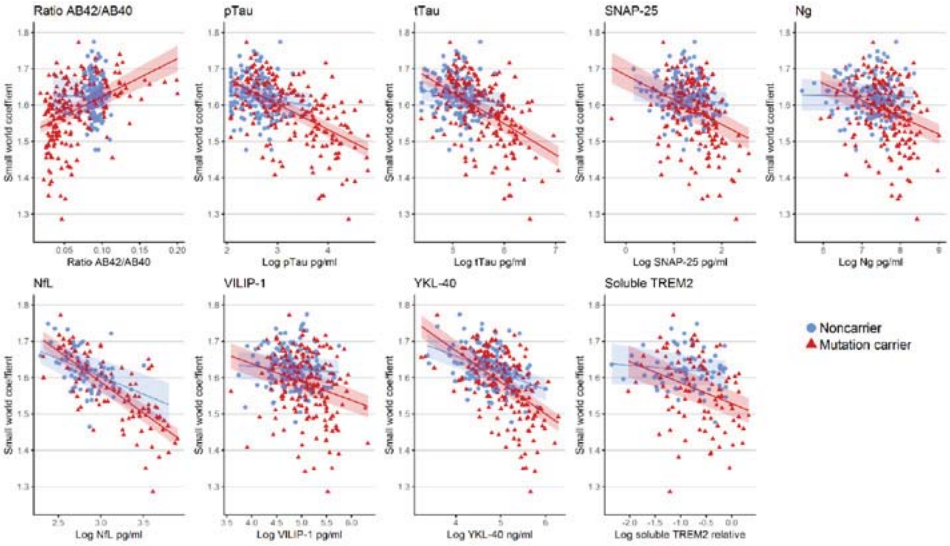

Figure 1 Associations between CSF biomarkers and grey matter networks for mutation carriers and noncarriers

Legend: Adjusted for sex. Prediction with 95% confidence intervals. sTREM2 = soluble TREM2 relative to a reference sample.

3.1 Associations between CSF biomarkers and the small world coefficient

Across the whole group, we found that all AD markers were related to alterations in grey matter networks (Table 2). Higher levels of NfL most strongly related to lower small world values (β±SE = -0.72±0.05; p<0.001), followed by YKL-40 (β±SE = -0.53±0.05; p<0.001), and pTau (β±SE = -0.53±0.05; p<0.001, Table 2). Models taking into account interaction terms of mutation status and CSF predictor, were significant for SNAP-25, Ng, pTau, tTau, NfL, VILIP-1 and YKL-40 (p<0.05, Fig. 1). Post-hoc comparisons showed that higher levels of SNAP-25 (-0.37 [CI 95%, -0.50,-0.24]) and Ng (-0.35 [CI 95%, -0.48,-0.21]), pTau (-0.58 [CI 95%, -0.69,-0.48]), tTau (-0.55 [CI 95%, -0.67,-0.44]) and VILIP-1 (-0.29 [CI 95%, -0.42,-0.16]) were related to lower small world values specifically in MCs. The association of higher NfL and YKL-40 and lower small world values was observed in both MCs and NCs, and this was stronger in MCs (NfL: MC = -0.76 [CI 95%, -0.89, -0.64] & NC = -0.44 [CI 95%, -0.77,-0.17]; YKL-40: MC = -0.61 [CI 95%, -0.72, -0.49] & NC = -0.32 [CI 95%, -0.48,-0.17]). When repeating models correcting for age, interaction effects for mutation status remained for SNAP-25, Ng, pTau, tTau, NfL and YKL-40 (p<0.05), but not for VILIP-1 (p=0.06). Next, we further studied in MCs whether the observed associations were specific to disease stage (Table S1, Fig. 2). No significant interaction terms with disease stage were observed, suggesting that associations of biomarkers and small world values were not specific to a certain stage.

Table 2 Associations between CSF markers and the small world coefficient

	Model 1 Predictor	Model 2 Mutation status* Predictor			Model 3 Mutation status* Predictor & adjustment for age		
Predictors	Predictor (beta)	Interaction (t)	Noncarriers (est slope)	Carriers (est slope)	Interaction (t)	Noncarriers (est adj slope)	Carriers (est adj slope)
$A\beta_{42/40}$ ratio	0.43 (0.05); p<0.001	1.8; p= 0.075	-0.01 (-0.47, 0.45); p=0.957	0.42 (0.31,0.52); p<0.001	1.9; p= 0.064	-0.18 (-0.57, 0.22); p=0.374	0.20 (0.11,0.30); p<0.001
pTau	-0.53 (0.05); p<0.001	-2.5; p= 0.014	-0.21 (-0.49, 0.07); p=0.144	-0.58 (-0.69, -0.48); p<0.001	-2; p= 0.047	0.06 (-0.18, 0.31); p=0.605	-0.39 (-0.49, -0.29); p<0.001
tTau	-0.48 (0.05); p<0.001	-3.1; p= 0.002	-0.16 (-0.38, 0.07); p=0.167	-0.55 (-0.67, -0.44); p<0.001	-2.6; p= 0.010	0.05 (-0.14, 0.24); p=0.596	-0.36 (-0.46, -0.26); p<0.001
SNAP-25	-0.33 (0.05); p<0.001	-2.1; p= 0.035	-0.13 (-0.31, 0.05); p=0.162	-0.37 (-0.50, -0.24); p<0.001	-2.2; p= 0.026	0.04 (-0.12, 0.19); p=0.645	-0.14 (-0.25, -0.02); p=0.019
Ng	-0.28 (0.05); p<0.001	-2.9; p= 0.004	-0.02 (-0.20, 0.16); p=0.836	-0.35 (-0.48, -0.21); p<0.001	-2.7; p= 0.008	0.07 (-0.07, 0.22); p=0.317	-0.20 (-0.31, -0.09); p=0.001
NfL	-0.72 (0.05); p<0.001	-2.2; p= 0.032	-0.44 (-0.71, -0.17); p=0.002	-0.76 (-0.89, -0.64); p<0.001	-3.7; P< 0.001	0.01 (-0.30, 0.32); p=0.940	-0.53 (-0.68, -0.38); p<0.001
VILIP-1	-0.26 (0.05); p<0.001	-2.0; p= 0.046	-0.05 (-0.24, 0.14); p=0.574	-0.29 (-0.42, -0.16); p<0.001	-1.9; p= 0.060	0.07 (-0.09, 0.22); p=0.401	-0.10 (-0.21, 0.01); p=0.078
YKL-40	-0.53 (0.05); p<0.001	-2.9; p= 0.004	-0.32 (-0.48, -0.17); p<0.001	-0.61 (-0.72, -0.49); p<0.001	-3.6; P< 0.001	0.05 (-0.11, 0.22); p=0.534	-0.30 (-0.43, -0.18); p<0.001
sTREM2	-0.33 (0.08); p<0.001	-2; p= 0.052	-0.08 (-0.33, 0.17); p=0.542	-0.40 (-0.61, -0.19); p<0.001	-1.3; p= 0.195	0.13 (-0.08, 0.34); p=0.229	-0.01 (-0.20, 0.18); p=0.912

Legend: All models were adjusted for sex; outcome = small world coefficient. sTREM2 = soluble TREM2 relative to a reference sample. All CSF markers, except the ratio are log-transformed.

3.2 Grey matter network and CSF biomarker trajectory by EYO

Finally, we estimated trajectories for all CSF and structural MRI markers according to EYO for the MCs, NCs, and the difference between MCs and NCs (Fig. 3; Table S2&3). Biomarker trajectories of the $A\beta_{42/40}$ ratio (EYO -18), $A\beta_{42}$ (EYO -16), pTau (EYO -18), tTau (EYO= -19), SNAP-25 (EYO= -15), Ng (EYO= -19) and VILIP-1 (EYO= -18) levels

were different in MCs as compared to NCs before differences were observed in grey matter networks (EYO= -8). NfL (EYO= -7) and YKL-40 (EYO= -7) trajectories were abnormal around the same time as grey matter networks, and sTREM2 (EYO= -3.5) and $A\beta_{40}$ (EYO= 0.5) showed abnormal levels in MCs compared to NCs later than grey matter networks.

4 Discussion

The main finding of our study is that CSF pathologic biomarkers showed associations with alterations in grey matter networks, and that axonal damage as measured with NfL showed the strongest relationship with worse grey matter network disruptions. Increased concentrations of the CSF markers for hyperphosphorylation of tau (pTau), neuronal injury and death (tTau and VILIP-1), and specific synaptic injury (SNAP-25 and Ng) were related to worse grey matter network organization in the MCs only. The observed associations were not dependent on staging based on a combination of the pTau/$A\beta_{42}$ ratio and the global CDR, suggesting that they were similar across disease development. According biomarker trajectories, most CSF markers showed abnormal levels before grey matter network abnormality in the MCs compared to the NCs, and for NfL and YKL-40 the timing was closest together with grey matter network alterations.

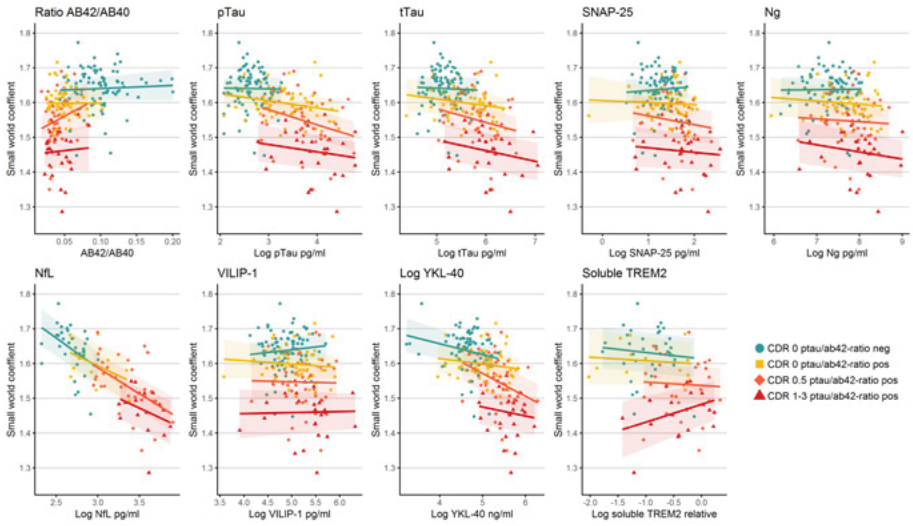

Figure 2 Associations between CSF biomarkers and grey matter networks within mutation carriers by disease stage

Legend: Adjusted for sex. Prediction with 95% confidence intervals. sTREM2 = soluble TREM2 relative to a reference sample.

So far, only the role of amyloid aggregation had been studied in relation to grey matter networks [14, 15]. Those findings suggested that grey matter networks are sensitive to brain structural changes related to amyloid aggregation in sporadic AD. Here, we found also that lower $A\beta_{42/40}$ ratios were associated with grey matter network disruptions. We further detected relationships between markers of other pathological processes in AD and grey matter network disruptions. The most pronounced association was observed for NfL, which suggests that loss of axonal integrity is an important factor for loss of grey matter network organization. The link between deterioration of grey matter covariance in AD to axonal tract damage supports the idea that grey matter covariance networks reflect, at least in part, axonal connectivity.

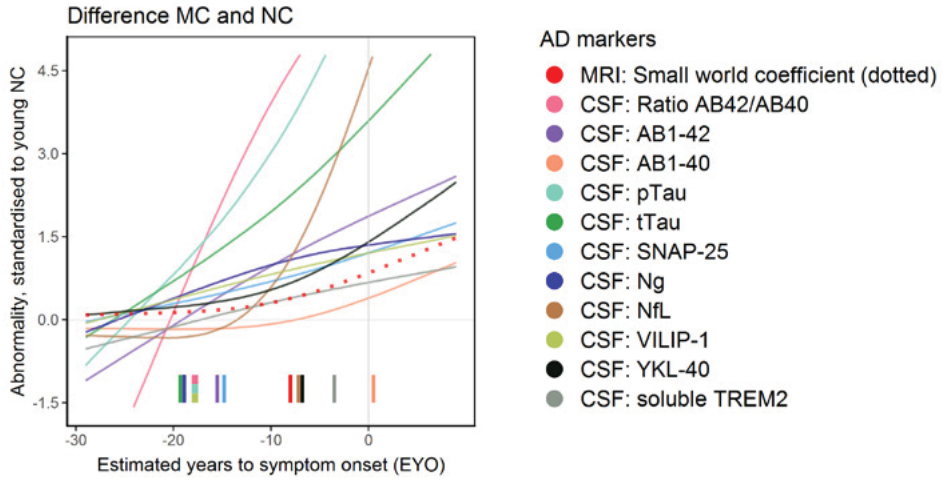

Figure 3 CSF and MRI biomarkers abnormality curves by EYO standardized to young noncarriers Legend: The graphs show the median estimated curves standardized to the noncarriers mean and standard deviation (Table 1). All fitted lines are the median of the mixed models with a cubic spline, family random intercept and sex as covariate, and for the small world coefficient also total grey matter volume. These analyses depend on sample sizes, which were for: small world N=439; $A\beta_{42}$, $A\beta_{40}$, pTau, tTau N = 352; SNAP-25, VILIP1 N=330, Ng & YKL-40 N=331, sTREM2 N=218; NfL N = 210. The tickmarks are the point that the 99% credible intervals of the difference between mutation carriers and noncarriers is different than 0.

We also observed that higher levels of the synaptic markers (SNAP-25 and Ng), hyper-phosphorylation (pTau) and neuronal damage (tTau and VILIP-1) were associated with grey matter network disruption, and this was specific for MCs. Synaptic damage in neurodegeneration could possibly influence brain connectivity in the opposite way as during brain development, when synaptic maturation and co-activation play a role in increasing brain connectivity [3]. The biomarker trajectories suggest that synaptic damage and neuronal loss precedes the changes we observe with MRI, therefore MRI changes could be a downstream effect. Recent analyses had already demonstrated that CSF pTau and tTau increases very early in the course of ADAD, in a more parallel

fashion with amyloid aggregation than according to hypothetical models [28]. The findings suggest that loss of connectivity structures at the microscale, in neurons, could lead to disrupted connectivity of the brain as measured on MRI. Longitudinal studies are needed to further examine the temporal relationship of these processes in more detail.

The associations between increased NfL and the astrocyte marker YKL-40 and network disruptions were also observed in NCs. Previous studies have shown that during aging NfL and YKL-40 levels increase [19, 23, 40, 41], and grey matter networks measure decline [42], though less pronounced than in predementia AD. Our findings suggest that also in non-AD related aging, loss of axonal integrity and inflammation may impact on grey matter network integrity. A next step to disentangle whether these are pathological processes that may render the brain more vulnerable for neurodegeneration and possibly reflect cognitive decline in normal and/or non-AD related aging. sTREM2, released by microglia, fluctuates over the course of AD, with an increase close to symptom onset [24, 43]. sTREM2 levels showed a complex relationship with grey matter networks, as the association disappeared in mutation carriers when analyses were corrected for age. The trajectory curves for sTREM2 showed changes a few years later than for grey matter networks, thus the inflammatory process, reflected by sTREM2 increases may not be directly related to the brain structure changes as captured by the grey matter networks.

A strength is that we studied the pathophysiology over the full course of AD. Investigating ADAD MCs of the DIAN study, along with NCs, was a powerful way for a parallel investigation of multiple disease processes that may contribute to grey matter network disruption. Due to the causative genes, the cross-sectional trajectory can inform longitudinal changes. Still, the reality is more complex [44], meaning further study in a longitudinal design is needed to understand of the drivers and downstream effect in disease progression of AD. A shortcoming of fitting AD biomarker trajectories over the expected years to symptom onset is that results in part depend on sample sizes and model assumptions. Most EYOs of divergence were similar to previous studies, except for Ng and YKL-40, which is an indication of the level of robustness across modeling methods [23]. In addition, the exact meaning of the biomarkers levels is not fully understood, and we were unable to investigate brain tissue as part of this study. Another limitation is that we assessed linear relationships between CSF and grey matter network values, which may underestimate existing relationships. Therefore, we evaluated whether patterns depended on disease severity, which may give rise to non-linear patterns. Still, some of those disease stage groups were of small size, and larger samples are required to further investigate these relationships in detail. Lastly, we studied a primary summary measure of network organization, which was a way to reduce the number of comparisons and increase the interpretability. The findings warrant follow-up research to further investigate, whether associations are specific for specific brain areas and network measures.

To summarize, loss of synaptic integrity and in particular axonal integrity as measured with increased NfL in CSF seems to be related to disrupted grey matter

network organization in ADAD. These findings suggest that normalization of neuronal injury or synaptic processes might lead to stabilization or improvement of grey matter network integrity.

References

1. He, Y., Z. Chen, and A. Evans, Structural insights into aberrant topological patterns of large-scale cortical networks in Alzheimer's disease. J Neurosci, 2008. 28(18): p. 4756-66.
2. Tijms, B.M., et al., Similarity-based extraction of individual networks from gray matter MRI scans. Cereb Cortex, 2012. 22(7): p. 1530-41.
3. Alexander-Bloch, A., J.N. Giedd, and E. Bullmore, Imaging structural co-variance between human brain regions. Nat Rev Neurosci, 2013. 14(5): p. 322-36.
4. Dai, Z. and Y. He, Disrupted structural and functional brain connectomes in mild cognitive impairment and Alzheimer's disease. Neurosci Bull, 2014. 30(2): p. 217-32.
5. Tijms, B.M., et al., Alzheimer's disease: connecting findings from graph theoretical studies of brain networks. Neurobiol Aging, 2013. 34(8): p. 2023-36.
6. Yao, Z., et al., Abnormal cortical networks in mild cognitive impairment and Alzheimer's disease. PLoS Comput Biol, 2010. 6(11): p. e1001006.
7. Li, Y., et al., Discriminant analysis of longitudinal cortical thickness changes in Alzheimer's disease using dynamic and network features. Neurobiol Aging, 2012. 33(2): p. 427 e15-30.
8. Pereira, J.B., et al., Disrupted Network Topology in Patients with Stable and Progressive Mild Cognitive Impairment and Alzheimer's Disease. Cereb Cortex, 2016. 26(8): p. 3476-3493.
9. Dicks, E., et al., Gray matter network measures are associated with cognitive decline in mild cognitive impairment. Neurobiol Aging, 2018. 61: p. 198-206.
10. Verfaillie, S.C.J., et al., A more randomly organized grey matter network is associated with deteriorating language and global cognition in individuals with subjective cognitive decline. Hum Brain Mapp, 2018. 39(8): p. 3143-3151.
11. Tijms, B.M., et al., Gray matter networks and clinical progression in subjects with predementia Alzheimer's disease. Neurobiol Aging, 2018. 61: p. 75-81.
12. Vermunt, L., et al., Grey matter networks decline over the disease course of autosomal dominant Alzheimer disease. in preparation.
13. Dicks, E., et al., Temporal trajectories of grey matter network measures across the Alzheimer's disease continuum and associations with cognitive decline. in preparation.
14. Tijms, B.M., et al., Gray matter network disruptions and amyloid beta in cognitively normal adults. Neurobiol Aging, 2016. 37: p. 154-160.
15. Voevodskaya, O., et al., Altered structural network organization in cognitively normal individuals with amyloid pathology. Neurobiol Aging, 2018. 64: p. 15-24.
16. Jack, C.R., Jr., et al., NIA-AA Research Framework: Toward a biological definition of Alzheimer's disease. Alzheimers Dement, 2018. 14(4): p. 535-562.
17. Fagan, A.M. and R.J. Perrin, Upcoming candidate cerebrospinal fluid biomarkers of Alzheimer's disease. Biomark Med, 2012. 6(4): p. 455-76.
18. Fagan, A.M., et al., Longitudinal change in CSF biomarkers in autosomal-dominant Alzheimer's disease. Sci Transl Med, 2014. 6(226): p. 226ra30.
19. Sutphen, C.L., et al., Longitudinal Cerebrospinal Fluid Biomarker Changes in Preclinical Alzheimer Disease During Middle Age. JAMA Neurol, 2015. 72(9): p. 1029-42.
20. Kester, M.I., et al., Cerebrospinal fluid VILIP-1 and YKL-40, candidate biomarkers to diagnose, predict and monitor Alzheimer's disease in a memory clinic cohort. Alzheimers Res Ther, 2015. 7(1): p. 59.
21. Preische, O., et al., Serum neurofilament dynamics predicts neurodegeneration and clinical progression in presymptomatic Alzheimer's disease. Nat Med, 2019. 25(2): p. 277-283.

22. Sutphen, C.L., et al., Longitudinal decreases in multiple cerebrospinal fluid biomarkers of neuronal injury in symptomatic late onset Alzheimer's disease. Alzheimers Dement, 2018. 14(7): p. 869-879.
23. Schindler, S.E., et al., Emerging cerebrospinal fluid biomarkers in autosomal dominant Alzheimer's disease. Alzheimers Dement, 2019. 15(5): p. 655-665.
24. Suarez-Calvet, M., et al., Early changes in CSF sTREM2 in dominantly inherited Alzheimer's disease occur after amyloid deposition and neuronal injury. Sci Transl Med, 2016. 8(369): p. 369ra178.
25. Ryman, D.C., et al., Symptom onset in autosomal dominant Alzheimer disease: a systematic review and meta-analysis. Neurology, 2014. 83(3): p. 253-60.
26. Bateman, R.J., et al., Clinical and biomarker changes in dominantly inherited Alzheimer's disease. N Engl J Med, 2012. 367.
27. Morris, J.C., The Clinical Dementia Rating (CDR): current version and scoring rules. Neurology, 1993. 43(11): p. 2412-4.
28. Schindler, S.E., et al., Cerebrospinal fluid biomarkers measured by Elecsys assays compared to amyloid imaging. Alzheimers Dement, 2018. 14(11): p. 1460-1469.
29. Gordon, B.A., et al., Spatial patterns of neuroimaging biomarker change in individuals from families with autosomal dominant Alzheimer's disease: a longitudinal study. Lancet Neurol, 2018. 17(3): p. 241-250.
30. Jack, C.R., Jr., et al., Update on the magnetic resonance imaging core of the Alzheimer's disease neuroimaging initiative. Alzheimers Dement, 2010. 6(3): p. 212-20.
31. Rubinov, M. and O. Sporns, Complex network measures of brain connectivity: uses and interpretations. Neuroimage, 2010. 52(3): p. 1059-69.
32. Watts, D.J. and S.H. Strogatz, Collective dynamics of 'small-world' networks. Nature, 1998. 393(6684): p. 440-2.
33. Humphries, M.D. and K. Gurney, Network 'small-world-ness': a quantitative method for determining canonical network equivalence. PLoS One, 2008. 3(4): p. e0002051.
34. Kang, J.H., et al., The Alzheimer's Disease Neuroimaging Initiative 2 Biomarker Core: A review of progress and plans. Alzheimers Dement, 2015. 11(7): p. 772-91.
35. Gaiottino, J., et al., Increased neurofilament light chain blood levels in neurodegenerative neurological diseases. PLoS One, 2013. 8(9): p. e75091.
36. Kleinberger, G., et al., TREM2 mutations implicated in neurodegeneration impair cell surface transport and phagocytosis. Sci Transl Med, 2014. 6(243): p. 243ra86.
37. Bittner, T., et al., Technical performance of a novel, fully automated electrochemiluminescence immunoassay for the quantitation of beta-amyloid (1-42) in human cerebrospinal fluid. Alzheimers Dement, 2016. 12(5): p. 517-26.
38. Mishra, S., et al., Longitudinal brain imaging in preclinical Alzheimer disease: impact of *APOE* epsilon4 genotype. Brain, 2018. 141(6): p. 1828-1839.
39. Carpenter, B., et al., Stan: A Probabilistic Programming Language. Journal of Statistical Software, 2017. 76(1): p. 1-29.
40. Bridel, C., et al., Diagnostic Value of Cerebrospinal Fluid Neurofilament Light Protein in Neurology: A Systematic Review and Meta-analysis. JAMA Neurol, 2019.
41. Alcolea, D., et al., Relationship between cortical thickness and cerebrospinal fluid YKL-40 in predementia stages of Alzheimer's disease. Neurobiol Aging, 2015. 36(6): p. 2018-23.
42. Chen, Z.J., et al., Age-related alterations in the modular organization of structural cortical network by using cortical thickness from MRI. Neuroimage, 2011. 56(1): p. 235-45.
43. Suarez-Calvet, M., et al., Early increase of CSF sTREM2 in Alzheimer's disease is associated with tau related-neurodegeneration but not with amyloid- pathology. Molecular Neurodegeneration, 2019. 14.
44. McDade, E., et al., Longitudinal cognitive and biomarker changes in dominantly inherited Alzheimer disease. Neurology, 2018. 91(14): p. e1295-e1306.

Supplemental data Chapter 4.2

Methods and materials

Table S1 Association of CSF markers with the small world coefficient within MCs by severity groups

	Within MCs: interaction of group and CSF predictor				
Predictors	Interaction (F)	Ratio negative (est slope)	Ratio positive & CDR 0 (est slope)	Ratio positive & CDR 0.5 (est slope)	Ratio positive & CDR 1-3 (est slope)
$A\beta_{42/40}$ ratio	0.63; p=0.59	0.03 (-0.13,0.20); p=0.68	0.0 (-0.36,0.35); p>0.99	0.44 (-0.14,1.02); p=0.13	0.09 (-0.53,0.71); p=0.77
pTau	0.68; p=0.57	-0.02 (-0.41,0.37); p=0.92	-0.17 (-0.4,0.05); p=0.13	-0.36 (-0.67,-0.06); p=0.02	-0.18 (-0.54, 0.19); p=0.34
tTau	0.34; p=0.8	-0.04 (-0.36,0.27); p=0.78	-0.13 (-0.35,0.1); p=0.27	-0.25 (-0.56,0.05); p=0.10	-0.2 (-0.52,0.12); p=0.23
SNAP-25	0.36; p=0.78	0.06 (-0.19,0.31); p=0.64	-0.03 (-0.24,0.17); p=0.75	-0.14 (-0.43,0.16); p=0.36	-0.07 (-0.34,0.2); p=0.61
Neurogranin	0.24; p=0.87	0.01 (-0.21,0.23); p=0.92	-0.07 (-0.3,0.16); p=0.53	-0.06 (-0.36,0.24); p=0.69	-0.15 (-0.47, 0.17); p=0.35
NfL log	0.16; p=0.92	-0.77 (-1.36,-0.18); p=0.01	-0.51 (-1.17,0.14); p=0.12	-0.67 (-1.04,-0.3); p<0.01	-0.50 (-1.26, 0.26); p=0.2
VILIP-1	0.30; p=0.83	0.09 (-0.15,0.33); p=0.46	-0.06 (-0.26,0.15); p=0.58	-0.02 (-0.3,0.26); p=0.89	0.02 (-0.25, 0.28); p=0.9
YKL-40	0.75; p=0.52	-0.22 (-0.45,0.02); p=0.07	-0.11 (-0.35,0.13); p=0.37	-0.46 (-0.84,-0.07); p=0.02	-0.18 (-0.66,0.3); p=0.46
sTREM2	0.82 ; p=0.48	-0.13 (-0.57,0.32); p=0.58	-0.07 (-0.5,0.36); p=0.74	-0.07 (-0.52,0.38); p=0.76	0.36 (-0.15,0.86); p=0.17

Legend: All models were adjusted for sex; outcome = small world coefficient. sTREM2 = soluble TREM2 relative to a reference sample. All CSF markers, except the ratio are log-transformed.

Details statistical methods of biomarker trajectory model:
The statistical model to fit biomarker trajectories by EYO, described by (Gordon, Blazey et al. 2018), allowed for non-linear effects by using a restricted cubic spline to model EYO, with knots on the 0.1, 0.5 and 0.9 of the distribution. The models had fixed terms for EYO, mutation status, their interaction and a random effect for family cluster. Models were adjusted for sex, and for the small world coefficient additionally for total grey matter volume. For the trajectories we used the biomarker data of the first available visit (Table S1 below). Model parameters were estimated with Hamiltonian Markov chain Monte Carlo sampling of the posterior distribution, with cauchy prior, 10,000 iterations in 8 chains, and thinning of 10 in the STAN and rstanarm package for R (Carpenter, Gelman et al. 2017). The EYO point of divergence is when the 99% credible intervals of the difference distribution between MCs and NCs did not overlap 0. We also provide the 95% and 99.5% of the credible intervals (Table S2).

R code: model_fit <- stan_glmer(standardized_biomarker_value ~ (1 | family_id) + eyo_1 + eyo_2 + mutation_status + eyo_term_1*mutation_status + eyo_term_2*mutation_status + sex, data = data, family = gaussian(), prior = cauchy(), prior_intercept = cauchy(), chains = 8, cores = 1, iter = 10000, thin = 10)

Table S2 Baseline values for biomarkers used for EYO in comparison to crossmodal data

	Noncarriers (NCs)	Noncarriers (NCs)	Mutation carriers (MCs)	Mutation carriers (MCs)
Grey matter network				
Small world coefficient	1.63 ± 0.05	1.62 ± 0.05	1.59 ± 0.09	1.59 ± 0.08
Traditional CSF markers				
$A\beta_{42}$ pg/ml	1,379 ± 464	1,407 ± 466	951 ± 635	974 ± 634
$A\beta_{40}$ pg/ml	15,491 ± 4490	15,698 ± 4418	1,4763 ± 4851	14,862 ± 4760
pTau pg/ml	14 ± 5	14 ± 5	32 ± 24	31 ± 23
tTau pg/ml	168 ± 56	169 ± 55	295 ± 169	290 ± 162
Ratio $a\beta_{42/40}$	0.088 ± 0.010	0.089 ± 0.010	0.065 ± 0.034	0.066 ± 0.035
Emerging CSF markers				
SNAP-25 pg/ml	3.6 ± 1.3	3.6 ± 1.3	4.6 ± 1.9	4.6 ± 1.9
Ng pg/ml	1,529 ± 736	1,563 ± 741	2303 ± 1186	2,297 ± 1,212
NfL pg/ml	820 ± 622	793 ± 544	1925 ± 1900	1,939 ± 1,762
VILIP-1 pg/ml	132 ± 52	133 ± 50	176 ± 78	174 ± 79
YKL-40 ng/ml	135 ± 66	133 ± 66	178 ± 92	173 ± 88
sTREM2, relative to reference sample	0.48 ± 0.22	0.47 ± 0.22	0.59 ± 0.29	0.58 ± 0.29

Legend: Light grey color are the values of table 1 for the main analysis of crossmodal comparison

Table S3 Estimated years to onset of divergence between mutation carriers and noncarriers

	EYO of divergence according 99% credible interval	EYO of divergence according 95% credible interval	EYO of divergence, according 99.5% credible interval
Grey matter network			
Small world coefficient	-8	-10.4	-7.5
Traditional CSF markers			
$A\beta_{42/40}$ ratio	-17.8	-18.4	-17.6
$A\beta_{42}$	-15.5	-16.4	-15.2
$A\beta_{40}$	0.5	-1	1.2
pTau	-17.7	-19.1	-17.2
tTau	-19.2	-20.4	-18.4
Emerging CSF markers			
SNAP-25	-14.8	-17.9	-12.6
Ng	-19	-20.1	-18.2
NfL	-7	-8.1	-6.7
VILIP-1	-17.9	-19.8	-16.8
YKL-40	-7	-10.1	-6
sTREM2	-3.5	-6.7	-2.2

Legend: These analysis depend on sample sizes, which were for: small world N=439; Aβ42, Aβ40, pTau, & tTau N = 352; SNAP-25 & VILIP1 N=330, Ng & YKL-40 N=331, sTREM2 N=218; NfL N = 210.

DIAN acknowledgements

Data collection and sharing for this project was supported by The Dominantly Inherited Alzheimer's Network (DIAN, UF1AG032438) funded by the National Institute on Aging (NIA), the German Center for Neurodegenerative Diseases (DZNE), Raul Carrea Institute for Neurological Research (FLENI), Partial support by the Research and Development Grants for Dementia from Japan Agency for Medical Research and Development, AMED, and the Korea Health Technology R&D Project through the Korea Health Industry Development Institute (KHIDI). This manuscript has been reviewed by DIAN Study investigators for scientific content and consistency of data interpretation with previous DIAN Study publications. We acknowledge the altruism of the participants and their families and contributions of the DIAN research and support staff at each of the participating sites for their contributions to this study.